NeuroImage: Clinical 32 (2021) 102880

Contents lists available at ScienceDirect

NeuroImage: Clinical

journal homepage: www.elsevier.com/locate/ynicl

Hemodynamic changes associated with common EEG patterns in critically ill patients: Pilot results from continuous EEG-fNIRS study

Ali Kassab [a,b], Dènahin Hinnoutondji Toffa [b], Manon Robert [b], Frédéric Lesage [c,d], Ke Peng [a,b,*], Dang Khoa Nguyen [a,b,e]

[a] Department of Neurological Sciences, Université de Montréal, C.P. 6128, succ. Centre-ville, Montreal, Quebec H3C 3J7, Canada
[b] Centre de Recherche du Centre Hospitalier de l'Université de Montréal, Université de Montréal, 900 Saint Denis St., Montreal, Quebec H2X 0A9, Canada
[c] Biomedical Engineering Institute, École Polytechnique de Montréal, 2500 Chemin de Polytechnique, Montréal, Quebec H3T 1J4, Canada
[d] Research Center, Montreal Heart Institute, 5000 Rue Bélanger, Montreal, Quebec H1T 1C8, Canada
[e] Division of Neurology, Centre Hospitalier de l'Université de Montréal, Université de Montréal, 1000 Saint Denis St, Montreal, Quebec (H2X OC1), Canada

ARTICLE INFO

Keywords:
Near-infrared spectroscopy
Cortical hemodynamic response
Status epilepticus
Burst suppression
Periodic discharge

ABSTRACT

Functional near-infrared spectroscopy (fNIRS) is currently the only non-invasive method allowing for continuous long-term assessment of cerebral hemodynamic. We evaluate the feasibility of using continueous electroencephalgraphy (cEEG)-fNIRS to study the cortical hemodynamic associated with status epilepticus (SE), burst suppression (BS) and periodic discharges (PDs). Eleven adult comatose patients admitted to the neuroICU for SE were recruited, and cEEG-fNIRS monitoring was performed to measure concentration changes in oxygenated (HbO) and deoxygenated hemoglobin (HbR). Seizures were associated with a large increase HbO and a decrease in HbR whose durations were positively correlated with the seizures' length. Similar observations were made for hemodynamic changes associated with bursts, showing overall increases in HbO and decreases in HbR relative to the suppression periods. PDs were seen to induce widespread HbO increases and HbR decreases. These results suggest that normal neurovascular coupling is partially retained with the hemodynamic response to the detected EEG patterns in these patients. However, the shape and distribution of the response were highly variable. This work highlighted the feasibility of conducting long-term cEEG-fNIRS to monitor hemodynamic changes over a large cortical area in critically ill patients, opening new routes for better understanding and management of abnormal EEG patterns in neuroICU.

1. Introduction

Continuous scalp electroencephalography (cEEG) monitoring is routinely used in the neurological intensive care unit (neuroICU) for diagnostic purposes, especially when suspecting nonconvulsive seizures (NCS) or nonconvulsive status epilepticus (NCSE) (Young and Mantia, 2017). The addition of functional neuroimaging techniques in clinical monitoring can further aid the diagnosis of NCSE (Hauf et al., 2009; Kutluay et al., 2005), as well as improving the understanding of the underlying pathophysiology (Siclari et al., 2013; Shimogawa et al., 2017). For example, animal studies of SE have reported increases in cerebral blood flow (CBF), oxygen pressure and metabolism (Lee et al., 2018), which showed that epilepsy or SE is not just an electrical disorder but also a vascular disorder. Unfortunately, in humans, only few reports have reported relative increase in cerebral blood flow (CBF) and cerebral blood volume (CBV) during SE using computer tomography perfusion (CTP) (Hauf et al., 2009), arterial spin labelling (Shimogawa et al., 2017), and single photon emission computed tomography (SPECT) (Kutluay et al., 2005). ^{18}Fluorodeoxyglucose positron emission tomography (^{18}FDG-PET) have shown both hypermetabolism (Siclari et al., 2013) and hypometabolism during SE (Strohm et al., 2019). Severe metabolic crisis has been described during SE (Vespa et al., 2007), and more recently, in new-onset refractory NCSE (Hurth et al., 2020).

In patients with refractory status epilepticus (RSE), EEG is also used to evaluate seizure control and anesthesia-induced background suppression (i.e. isoelectric or burst-suppression patterns) (Brophy et al., 2012). Achieving such patterns is commonly sought as an electrophysiological endpoint in RSE (Brophy et al., 2012) and intracranial

* Corresponding author at: CRCHUM, 900 Saint-Denis St, Montreal, Quebec H2X 0A9, Canada.
E-mail addresses: ali.kassab@umontreal.ca (A. Kassab), denahintoffa@gmail.com (D. Hinnoutondji Toffa), manon.robert.chum@ssss.gouv.qc.ca (M. Robert), frederic.lesage@polymtl.ca (F. Lesage), ke.peng@umontreal.ca (K. Peng), d.nguyen@umontreal.ca (D. Khoa Nguyen).

https://doi.org/10.1016/j.nicl.2021.102880
Received 15 June 2021; Received in revised form 4 November 2021; Accepted 5 November 2021
Available online 8 November 2021

hypertension (Marshall et al., 2010). However, the neuroprotective role of pharmacologically induced BS in the setting of acute brain injury remains debated. Some studies have suggested that BS lowers brain metabolism, which could be beneficial in situations where CBF and oxygen delivery are compromised such as during prolonged seizures (Ching et al., 2012; Doyle and Matta, 1999). Conversely, other studies have found that the brain is in a state of relative hyperexcitability during BS because inhibitory post-synaptic potentials are completely suppressed while excitatory potentials are only partially diminished. In this state of relative cortical excitability, even subliminal stimuli can elicit bursts of whole-brain activity in animal studies, a phenomenon closely resembling SIRPIDS (stimulus-induced rhythmic, periodic, or ictal discharges), a common EEG phenomenon in the critically ill (Ferron et al., 2009). Whichever the case may be, there is little doubt that functional neuroimaging techniques provide valuable information regarding the neurophysiological dynamics of medically induced BS patterns. The study of vascular changes and neurovascular coupling during BS reveals the ability of the brain in responding to spontaneous or externally stimuli, which may help further delineate the putative neuroprotective role in critically ill patients (Berndt et al., 2021).

The increased use of cEEG in the neuroICU has also led clinicians to recognize EEG patterns belonging to the ictal-interictal continuum (IIC) (Pohlmann-Eden et al., 1996), including generalized periodic discharges (GPDs) and lateralized periodic discharges (LPDs). While both GPDs and LPDs are commonly observed in the neuroICU, their clinical significance remains controversial as to whether they truly represent an ictal phenomenon or not (Cormier et al., 2017). Specifically, LPDs were reported to be usually associated with hypermetabolism (Struck et al., 2016), however, both hypo- and hypermetabolism have been observed during GPDs (Bansal et al., 2016). Clinical functional neuroimaging monitoring of the hemodynamic changes during IIC patterns may serve as an adjunct modality for clinicians to identify potential oxygen undersupply and neuronal damage, which necessitate more aggressive treatment to the patients (Herlopian et al., 2018).

Despite these potentials, conventional non-invasive neuroimaging approaches (e.g., PET, SPECT) are limited by practical aspects in this context and by their temporal resolution whereas invasive methods (e.g., invasive brain tissue oximetry, invasive monitoring of cerebral perfusion pressure) carry risks of medical complications and provide a limited spatial view. Functional near-infrared spectroscopy (fNIRS) is a non-invasive optical neuroimaging technique that reconstructs cortical hemodynamic conditions (in terms of concentration changes of oxyhemoglobin, HbO and deoxyhemoglobin, HbR) from attenuation of near-infrared light during its propagation within the cortex (Scholkmann et al., 2014). Compared with other functional neuroimaging modalities, fNIRS provides long-term continuous measurement of cortical oxygenation at a relatively high temporal resolution (up to the order of 0.01 s), making it suitable as a low-cost portable neuromonitoring technique in the neuroICU (Pisano et al., 2020). The use of fNIRS to investigate SE (Diaz et al., 2006; Giorni et al., 2009; Haginoya et al., 2002; Martini et al., 2019; Monrad et al., 2015) has been limited to a few cases reports conducted in young children with thin skull. Moreover, most of those studies have only employed a couple of optodes covering the forehead. Simultaneous EEG was not always present, and recording sessions were typically short in duration (<1 h). To date, investigation of BS with fNIRS has only been performed in neonates (Chalia et al., 2016; Connolly et al., 2015; Roche-Labarbe et al., 2007) and no study has yet investigated PDs using fNIRS or other optical imaging methods.

In this work, we conducted for the first time prolonged cEEG-fNIRS recordings over a large cortical area in critically ill patients admitted to the neuroICU. We extracted the cortical hemodynamic response to each type of the recorded EEG events, which included NCSE, PDs and pharmacologically induced BS patterns. The goals of this study were twofold: we aimed to 1- assess the feasibility of performing long-term cEEG-fNIRS in comatose patients in neuroICU; and 2- to provide first evaluation of the hemodynamic responses associated with each electroclinical condition, relating the characteristics of those changes to the type or duration of the events.

2. Material and methods

2.1. Patients

This study was approved by the Institutional Review Board at the University of Montreal Hospital Center (CHUM). Eleven neuroICU patients (seven males, age range: 31 to 61 years) with seizures or SE were recruited. At admission, the patients were diagnosed with SE (n = 7) or acute encephalopathy (n = 4). Written informed consent was obtained from legally authorized representatives. An overview of our study procedures is depicted in Fig. 1.

2.2. cEEG-fNIRS data acquisition

A portable EEG-fNIRS system previously developed and validated by our group (Kassab et al., 2018) was used in this study. 19 EEG electrodes were mounted following the International 10–20 layout. For the fNIRS part, the system allows the installation of up to 32 light emitters and 32 detectors, which form a maximum of 128 fNIRS channels operating at 735 nm and 850 nm. Three previously validated full-head EEG-fNIRS caps (small, medium and large) (Kassab et al. 2018) were utilized in this study to fit different sizes of patient's head. A base optode montage consisting of rows of sources alternating with rows of detectors was designed for neuroICU patients kept in a supine position which covered most of the frontal lobe, the central areas, the bilateral temporal lobe and the anterior portion of posterior regions. Depending on the actual head shape, size, the presence of skin lesions on the scalp and the location of observed epileptiform activities, the optode layout for each patient was modified from the base montage to maintain an optimal coverage. The distance between an fNIRS light emitter and a light detector that formed a channel was kept within 2.5 cm to 5 cm. If needed, a dark elastic woolen fabric was placed over the cap to improve probe-tissue contact and to reduce ambient light. The acquired EEG data and fNIRS data were sampled at 500 Hz and 20 Hz respectively.

2.3. Data processing and analysis

2.3.1. EEG identification of seizures, PDs and BS and EEG data analysis

EEG data were independently reviewed by two epileptologists (DHT and DKN) to label and confirm interictal epileptiform discharges, PDs, as well as electrical onsets and offsets of seizures, bursts and suppression periods. The American Clinical Neurophysiology Society's (ACNS) diagnostic criteria were used for the diagnosis of electrographic and electroclinical seizures (Hirsch et al., 2013). The diagnosis of NCSE was based on both EEG and clinical data following the modified Salzburg Consensus Criteria (mSCNC) (Leitinger et al., 2019). Quantitative EEG analysis was performed offline for the whole EEG recording using Persyst 13 EEG software (Persyst Systems, Arizona, USA), including rhythmicity spectrogram, fast Fourier transform (FFT) spectrogram, asymmetry relative spectrogram, and amplitude EEG spectrogram (for parameters, see Table 1).

2.3.2. fNIRS data pre-processing

For each patient, an analysis period representative of the whole recording was selected based on the type and number of presented events, number of valid channels and noise levels. The selected fNIRS data were processed with open-source toolbox Homer2 (Huppert et al., 2009) and in-house developed scripts. fNIRS channels with an intensity of <100 (AU) or a signal-to-noise ratio of <2 were excluded from further analysis. For the remaining channels, raw optical data were first converted into optical density changes. A principal component analysis (PCA) filter that removed 90% of the global variance across channels was applied to mitigate motion artifacts and the interferences from

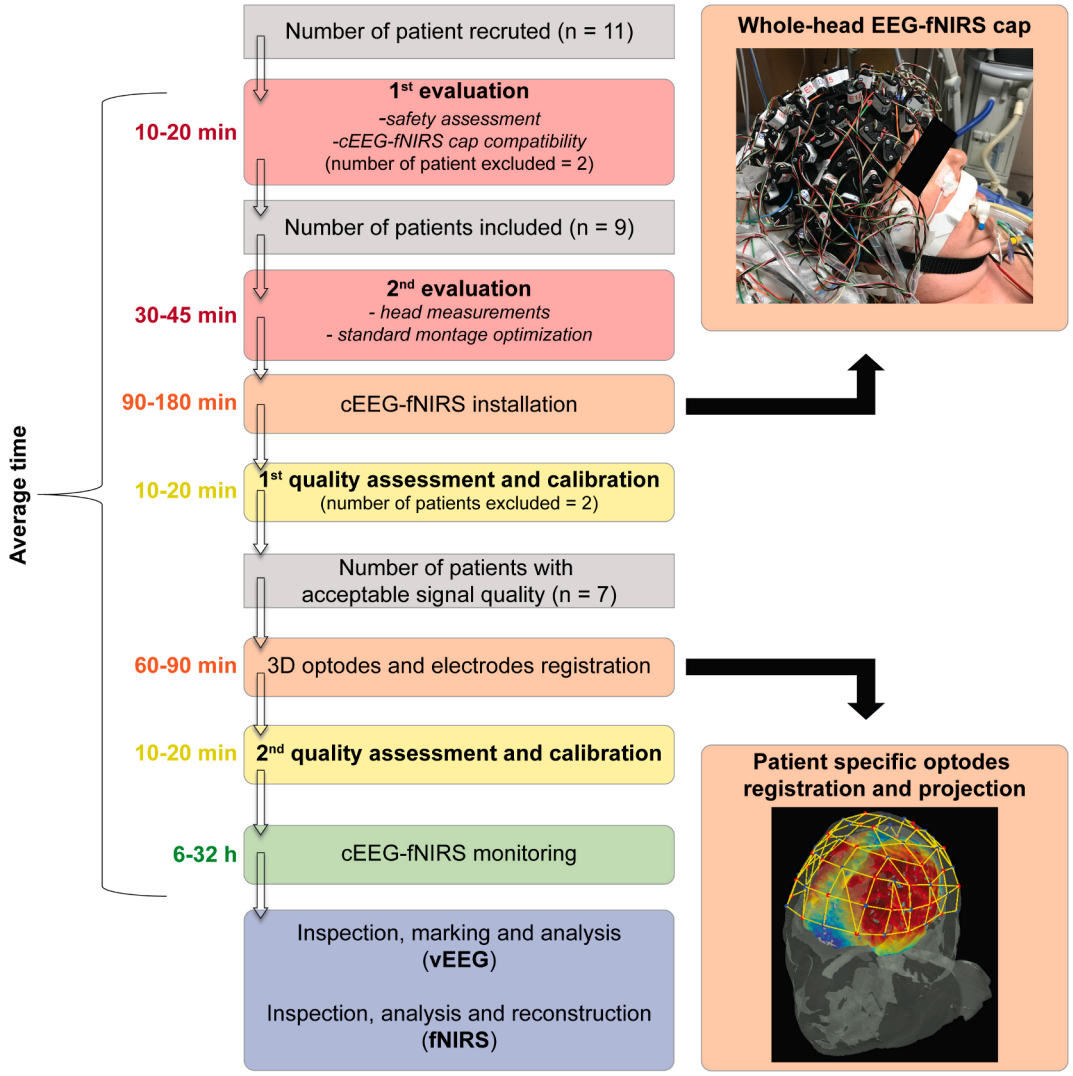

Fig. 1. Sketch plot of the patient evaluation, continuous encephalography and functional near-infrared spectroscopy data acquisition, and data analysis procedures.

superficial layers (e.g., scalp, skin and skull) (Virtanen et al., 2009; Zhang et al., 2005) . For comatose patients in the neuroICU, motion artifacts may come from mattress air pressure fluctuations and routine care procedures performed by medical staff. A Homer2 automatic algorithm based on signal standard deviation and amplitude change was then used to further check for remaining motion artifacts. Any EEG event within the time period from 30 s prior to a motion artifact to 30 s after the artifact was rejected. The remaining EEG events were then manually inspected to ensure no event mislabeling. The fNIRS optical density time courses were passed to a 3rd order Butterworth bandpass filter with cutoff frequencies at 0.01 Hz and 0.20 Hz, and were then transformed into concentration changes in HbO and HbR using the modified Beer-Lambert Law with a partial pathlength factor of 6. The concentration changes in HbT were calculated by a direct sum of HbO and HbR changes.

2.3.3. *Extraction of hemodynamic response functions*

The estimation of hemodynamic response function (HRF) to each type of EEG patterns/event was conducted through an event-related general linear model (GLM) analysis. We employed a bin approach similar to that used by Chalia et al. (2016), which was to group each type of EEG event into 5-second width bins of different durations. For instance, seizures lasted<20 s were divided into four bins: [0 to 5 s], [5 s to 10 s], [10 s to 15 s] and [15 s to 20 s]. These bins were treated as distinct conditions in the following GLM analysis, allowing their associated responses to vary freely from the others. Considering the intrinsic delay of hemodynamic changes relative to the underlying electrical activity, we modeled the hemodynamic response to a particular bin of events from 5 s before the EEG onset to 15 s after the EEG offset of the longest possible event within the bin (e.g., the response to the bin of seizures from 15 to 20 s was modeled from 5 s before the seizure onset shown on EEG to 35 s after the EEG onset, i.e., 15 s after the offset of the longest 20-sec seizure). The functions used in the GLM were consecutive Gaussian functions with a standard deviation of 1 s and a step size of 1 s as well. After the extraction, each HRF was normalized using the mean amplitude from 2 s before the event EEG onset to the event onset as the baseline level.

To enable comparisons between conditions, we generated a representative HRF corresponding to each bin and each event type of each patient. This was conducted by performing a PCA on the HRFs of all available channels, reconstructing the HRFs with the components that accounted for at least 80% of global variance, and averaging new HRFs across channels. Including only the principal components allows us to focus on the hemodynamic changes that were most prominent across brain regions, as well as to reduce the possibility of including spurious local signals in the representative HRF. A similar PCA-based extraction method was used by Chalia et al. (2016). More specifically, the original HRFs were first pre-centered to zero-mean, and were aligned as an $t \times p$

Table 1
Study characteristics and clinical details for each patient.

Patient (sex, age, BMI)	Admission Dx (cEEG-fNIRS MNT start)	# cEEG-fNIRS MNT sessions (analyzed time)	Neurologic status	Cardio-respiratory status	Vital signs MNT (mean ± SD)	AEDs, anesthetics	Anatomical neuroimaging	Outcome
P1 (F, 31, 40.7)	PSE (5 days)	4 sessions, 31.5 h (68 min)	Comatose	ACV (on inotropes)	MAP: 92 ± 15 mmHg T°: 37 ± 1 °C SpO_2: 100 ± 0 % $EtCO_2$: 34 ± 1 mmHg Glycemia: 7.0 ± 0.7 mmol/L RASS: −2 ± 1	Propofol, MDZ, TP, CTP, CBZ, PHT	Surgical cavity	Discharged at 15 days Mild clinical improvement (refractory epilepsy)
P2 (M, 50, 23.7)	Pneumonia, CPA, RCSE (same day)	2 sessions, 5.5 h (49 min)	Comatose	ACV (on inotropes)	MAP:82 ± 5 mmHg T°: 37.6 ± 0.2 °C SpO_2: 99 ± 0 % $EtCO_2$: 44 ± 2 mmHg Glycemia: 13.4 ± 1 mmol/L RASS: −5 ± 0	Propofol, MDZ, LEV	T2/FLAIR hyperintensities	Discharged at 9 days IHT
P3 (F, 52, 33.4)	NCSE (4 days)	1 session, 4.5 h (99 min)	Comatose	ACV (no inotropes)	MAP: 103 ± 6 mmHg T°: 36.8 ± 0.2 °C SpO_2: 98 ± 2 % $EtCO_2$: 34 ± 2 mmHg Glycemia: 5.0 ± 0.3 mmol/L RASS: −5 ± 0	Propofol, MDZ, LSM, LEV, PHT	Surgical cavity, hypodensity	Discharged at 4 days IHT
P4 (M, 57, 35.5)	GI bleeding, TME, CSE, NCSE (7 days)	2 sessions, 7 h (97 min)	Comatose	ACV (on inotropes)	MAP: 88 ± 9 mmHg T°: 36.7 ± 0.3 °C SpO_2: 100 ± 0 % $EtCO_2$: 34 ± 1 mmHg Glycemia: 7.0 ± 0.7 mmol/L	Propofol, LEV, LSM	Restricted diffusion, T2/FLAIR hyperintensities	Decd at 22 days
P5 (M, 40, 23.1)	SE, HE/SREAT (26 days)	3 sessions, 8 h (197 min)	Comatose	ACV (no inotropes)	MAP: 76 ± 4 mmHg T°: 37.5 ± 0.1 °C SpO_2: 99 ± 1 % $EtCO_2$: 35 ± 2 mmHg Glycemia: 5.4 ± 0.6 mmol/L RASS: −5 ± 0	Propofol, MDZ, LEV, PHT	Normal	Discharged at 155 days VS
P6 (M, 45, 17.6)	CSE, RNCSE (2 days)	5 sessions, 10.5 h (261 min)	Comatose	ACV (on inotropes)	MAP: 70 ± 4 mmHg T°: 37.5 ± 0.2 °C SpO_2: 97 ± 3 % $EtCO_2$: 37 ± 3 mmHg Glycemia: 7.7 ± 1.2 mmol/L RASS: −5 ± 0	Propofol, MDZ, LSM, LEV, TP, CBZ, CLB	Cortical and sub-cortical thickening, T2/FLAIR hyperintensities	Discharged at 87 days Mild clinical improvement (persistence of short seizures)
P7 (M, 34, 21.3)		3 sessions, 8.5 h (140 min)	Comatose	ACV (on inotropes)	MAP: 75 ± 7 mmHg			Discharged at 50 days

(*continued on next page*)

Table 1 (*continued*)

Patient (sex, age, BMI)	Admission Dx (cEEG-fNIRS MNT start)	# cEEG-fNIRS MNT sessions (analyzed time)	Neurologic status	Cardio-respiratory status	Vital signs MNT (mean ± SD)	AEDs, anesthetics	Anatomical neuroimaging	Outcome
	R hemiparesis, global aphasia, NCSE (3 days)				T°: 37.5 ± 0.2 °C SpO_2: 100 ± 0 % $EtCO_2$: 41 ± 3 mmHg Glycemia: 4.7 ± 0.5 mmol/L RASS: −5 ± 0	Propofol, MDZ, LSM, LTG, LEV, PHT	Surgical cavity, restricted diffusion, T2/FLAIR hyperintensities	Significant clinical improvement (strength and speech)

Abbreviations. M: male, F: female, MNT: monitoring, BMI: body mass index, AEDs: antiepileptic drugs, ACV: assisted controlled ventilation, CT: cortical thickness, SK: skull thickness, SE: standard error, SD: standard deviation, MAP: mean arterial pressure, T°: mean temperature, SpO_2: mean oxygen saturation, $EtCO_2$: mean end-tidal carbon dioxide, RASS: mean Richmond Agitation and Sedation Scale value, R: right, PSE: partial status epilepticus, CSE: convulsive status epilepticus, NCSE: non-convulsive status epilepticus, RCSE: refractory convulsive status epilepticus, RNCSE: refractory nonconvulsive status epilepticus, CPA: cardio-pulmonary arrest, TME: toxico-metabolic encephalopathy, HE: Hashimoto encephalopathy, SREAT: steroid-responsive encephalopathy associated with autoimmune thyroiditis, CBZ: carbamazepine, CLB: clobazam, CTP: citalopram, LEV: levetiracetam, LCM: lacosamide, LTG: lamotrigine, MDZ: midazolam, PHT: phenytoin, TPM: topiramate, CMB: cerebral microbleed, DCA: diffuse cerebral atrophy, VS: vegetative state, Decd: deceased, IHT: inter-hospital transfer, N/A: not available.

HRF matrix $\boldsymbol{H}$ where t is the number of time points in the HRF and p is the number of available channels. PCA was conducted by performing an eigendecomposition on the covariance matrix $\boldsymbol{C} = \boldsymbol{H}^{\mathrm{T}}\boldsymbol{H}/(\text{t-1})$, i.e.

$$C = VLV^T$$

where $\boldsymbol{V}$ is a matrix of eigenvectors with each column being one eigenvector, $\boldsymbol{L}$ is a diagonal matrix with eigenvalues λ_i, $i = 1, 2, \cdots, p$, on the diagonal in descending order. The principal components $\boldsymbol{R}$ of matrix $\boldsymbol{H}$ were given by:

$$\boldsymbol{R} = \boldsymbol{HV}$$

In this study, we only kept the principal components that accounted for ≥ 80% of the variance, i.e. we created a new $\boldsymbol{R}$' :

$$\begin{cases} R'_{j,k} = 0, for j = 1, 2, \cdots, tandk = s, s+1, \cdots, p \\ R'_{j,k} = R_{j,k}, otherwise \end{cases}$$

where s was determined by

$$\frac{\sum_{i=s}^{p}\lambda_i}{\sum_{i=1}^{p}\lambda_i} \le 0.2 and \frac{\sum_{i=s-1}^{p}\lambda_i}{\sum_{i=1}^{p}\lambda_i} > 0.2$$

A new HRF matrix $\boldsymbol{H}$' was then generated by:

$$\boldsymbol{H}' = \boldsymbol{R}'\boldsymbol{V}^T$$

Finally, we added each channel's DC component that was removed in data pre-centering back to the new channel HRF (i.e., each column of $\boldsymbol{H}'$). The representative HRF was then obtained by a simple averaging of the new HRFs (with DC) across available channels.

To ensure that the extracted representative HRFs were synchronized with the EEG events and to assess the strength of the responses, we presented a confidence level for each representative HRF by employing a surrogate timecourse approach (Peng et al., 2016). Briefly, we took the hemoglobin concentration change time courses of all available fNIRS channels of a patient, performed a fast Fourier Transform on each channel time course, and randomized the phases of the frequency components. Specifically, the same set of randomized phases for frequency components was applied to all the channels. The frequency components with randomized phases of a channel were then re-transferred to the time domain to generate a surrogate time course. Note that by using the phase randomization method, we aimed to maintain the same signal autocorrelation of a channel as in the original timecourse, and by applying the same set of randomized phase set to all the channels, we intended to keep similar covariance structure among different channels. The surrogate timecourses of all channels were then passed to the GLM model and the PCA procedures to produce a spurious representative HRF. The same randomization and extraction process was repeated 100 times for each true representative HRF. The peak amplitude (PA) of the true representative HRF was then compared to the amplitude values during the same time period of all 100 spurious representative HRFs to evaluate the possibility of the peak being generated by chance or noise. More specifically, we approximated the 100 amplitude values of the spurious representative HRFs with a normal distribution, and reported the confidence level of the true representative HRF by calculating the ratio of the tail area marked by the PA of the true representative HRF on the normal distribution relative to the entire area of the distribution. Therefore, the ratio is a scalar value between 0 and 1, and a smaller ratio indicated higher response strength and a less chance of the true representative HRF being generated by pure noise or other artifacts in data processing. For a representative HRF of a bin, the PA was defined as the mean value averaged from 1 s before the maximum value of a main peak following the EEG onset of the event (or the minimum value if a nadir was detected) to 1 s after the maximum value.

2.3.4. Cortical projection of hemoglobin concentration changes

The projection of hemoglobin concentration changes back onto the cortical surface was carried out using the toolbox AtlasViewer (Aasted et al., 2015) integrated in Homer2. For each patient, the included optical sources and detectors were first co-registered onto the Colin27 five-layer brain atlas. A forward model was computed using the Monte-Carlo algorithm that simulated the migration of 100 million photons at each optical source and detector. The produced sensitivity matrix was used to solve the regularized inverse problem and to generate voxel-wise concentration changes (Custo et al., 2010). For each bin of events, the time period of concentration changes to be displayed on the cortex was selected to be the PA of the HbO representative HRF. We chose HbO over HbR in this study as previous work has generally reported a much higher signal-to-noise ratio in HbO responses than HbR responses (Obrig et al., 2000; Yennu et al., 2016). A threshold of extent was imposed to the generated spatial concentration change images to only keep the cortical areas where the detection sensitivity was high than −2dB. It should be noted that the projections of fNIRS-measured hemoglobin concentration changes were limited by the imaging depth, cortical coverage and the detection sensitivity. Therefore, our interpretation of the hemodynamic response spatial features was only based on the brain areas where a relatively high sensitivity was obtained (see Fig. S2 for examples of sensitivity map).

2.3.5. Statistical analysis

To further explore the relationship between detected EEG events and the characteristics of the corresponding hemodynamic responses, we

established a linear mixed-effect regression model modeling event duration with fixed effect for response peak amplitude (PA) or response full-width-at-half-maximum (FWHM) and uncorrelated random effect for intercept (grouped by patients) and residual:

$$\boldsymbol{y} = \beta_0 + \beta_1 {}^{*}\boldsymbol{d} + \boldsymbol{z}^{*}\boldsymbol{u} + \boldsymbol{\varepsilon}$$

where $\boldsymbol{y}$ is an N by 1 vector containing the PAs or FWHM extracted from bin representative HRFs of a certain type of EEG event across all M patients where the type of event was detected; $\boldsymbol{d}$ is an N by 1 vector of the maximum event duration of the bins, $\boldsymbol{z}$ is an N by M random effect design matrix where

$$\begin{cases} z_{n,m} = 1, if\, y_n is from patient m; \\ z_{n,m} = 0, otherwise \end{cases}$$

$\boldsymbol{u}$ is the corresponding M by 1 random effect variable vector, and ε is the uncorrelated N by 1 model residual vector. We assume $u_m\ N(0, \sigma_u^2)$ and $\varepsilon_n\ N(0, \sigma_\varepsilon^2)$. For a representative HRF of a bin, the PA was defined as mentioned in the above section, and the FWHM was defined as the length of the time during which the response was larger than half of the PA (or during which the response was smaller than half of the nadir amplitude). In this study, PA was used to assess the hemodynamic response intensity and the FWHM was chosen to assess the duration of the response.

The goodness of fit of the regression models was evaluated through the calculation of the p-value of an F-test on the fixed effect regression coefficients, as well as the R-squared and the adjusted R-squared values. Specifically,

$$R^2 = \frac{SSR}{SST} = 1 - \frac{SSE}{SST}, and$$

$$adjusted R^2 = 1 - \frac{SSE/(N-l-1)}{SST/(N-1)}$$

where SST is the total sum of squares $SST = \sum_{m=1}^{M}\sum_{n_m=1}^{N_m}\left(y_{n_m} - \bar{y}_m\right)^2$,

SSR is the regression sum of squares $SSR = \sum_{m=1}^{M}\sum_{n_m=1}^{N_m}\left(\hat{y}_{n_m} - \overline{\hat{y}_m}\right)^2$,

and SSE is the error sum of squares SSE = SST - SSR. $\hat{y}$ contains the predicted conditional PA or FWHM values using both fixed and random effects of the model. L = 1 is the number of fixed effect variable in the model.

3. Results

3.1. Patient clinical information

Four patients were excluded at the initial quality assessment stage due to the use of intracranial probes (n = 1), a recent craniotomy/cranioplasty (n = 1), and poor optical signal quality (n = 2). The clinical information of the remaining seven patients (five men, age = 44 ± 10 years) is included in Table 1. Fig. 2 presents structural and electrophysiological findings with structure image slices and representative EEG clips selected from each patient. Table 2 summarizes the main electrophysiological and optical findings. The details of the neuroICU care and the collected vital sign signals are shown in Fig. S1.

3.2. Hemodynamic changes associated with NCS in NCSE

NCSE was identified from EEG in three patients (P2, P4 and P6). In addition, Patient P1 showed seizure-like activities including bursts of spikes and bursts of fast activities. The representative HRFs to bursts of spikes, bursts of spikes plus and bursts of fast activities all showed large increases in HbO and HbT, and a delayed HbR increase (Fig. 3A). The associated HbO/HbT increases and HbR decreases were seen to be relatively short which was as expected considering the briefness of the bursts (mostly < 2 s). In Patients P2, P4 and P6, a total of 199 seizures with a mean duration of 16.6 s and a standard deviation of 20.4 s were recorded and analyzed. Among them, over 88% of the seizures lasted<25 s. These seizures formed bins that contained at least three samples in our event-related analysis. In this section, we present the representative HRFs and the cortical projections of hemoglobin concentration changes from bins of seizures<25 s. On the other hand, bins of seizures with durations > 25 s usually did not contain many samples for analysis (i.e. < 3) and were not always present across patients. These bins of longer seizures were treated as events of non-interest in each patient's GLM to control their potential confounding effect in the estimation of the hemodynamic response to other events that were temporally overlapped or adjacent. The results of long seizures are therefore not shown here. In all of the three patients, the representative HRFs showed an overall increase in HbO concentration with mean PA of 0.067 ± 0.026 μM averaged across patients, an increase in HbT (mean PA = 0.061 ± 0.029 μM) and a decrease in HbR (mean nadir amplitude = -0.028 ± 0.021 μM) following the onset of an NCS (Fig. 3B–D). These changes returned to baseline at around 10 s after the offset of the NCS. Linear mixed-effects models modelling seizure duration with fixed effects for response PA failed to report significant correlation for any of the hemoglobin types at $\alpha = 0.05$ (Fig. 4A). However, the relation between seizure duration and response FWHM was statistically significant for HbO with $p = 0.021$ and adjusted R-squared value = 0.569 and for HbT with $p = 0.034$ and adjusted R-squared value = 0.403 (Fig. 4B), showing a positive correlation between the lengths of EEG evidence of seizures and the durations of associated hemodynamic changes. An initial dip characterized mainly by a large decrease in HbO at the beginning of the response was observed in Patients P4 (Fig. 3C, see orange arrows on the representative HRF plots) and P6 (Fig. 3D, see black arrows).

For each patient, cortical projection of the hemoglobin concentration changes revealed brain regions that showed a highest level of magnitude in the HbO response to NCS. These regions were in most cases concordant with structural findings and electrophysiological results (Table 2, comparison of electrophysiological and optical findings). Moreover, hemodynamic activity in the contralateral region was also noticed in our patients. Examples included Patient P1 whose burst of spikes and fast activities were mostly identified in the right fronto-centro-temporal area on scalp EEG but showed large HbO increases in the left frontal, central and temporal regions together with right side activations (Fig. 3A Cortical projections), as well as Patients P2 and P6 on whom seizures affected more the EEG signals over the left frontocentral area but were seen to be associated with hemodynamic activations with nearly symmetrical spatial profiles in the corresponding regions of both hemispheres (Fig. 3B and D Cortical projections).

3.3. Hemodynamic changes associated with BS

BS patterns were observed in four patients (Patients P3, P5, P6, P7). Using the hemoglobin concentration during suppression periods as baseline, we observed increases in HbO (mean PA = 0.079 ± 0.058 μM) and HbT (mean PA = 0.067 ± 0.046 μM) and decreases in HbR levels (mean nadir amplitude = -0.027 ± 0.019 μM) following the onset of bursts in the representative HRFs of all those patients, see Fig. 5. Similar to NCS-related responses, the duration and amplitudes of these changes were positively correlated with the lengths of the bursts (Fig. 6), with $p = 0.000078$ and $p = 0.0096$ and for the HbO PA and FWHM, $p = 0.00017$ and $p = 0.000089$ for HbR nadir amplitude and FWHM, and $p = 0.00023$ and $p = 0.00024$ for HbT PA and FWHM.FWHM, and $p = 0.018$ for a negative correlation between HbR nadir amplitude and burst duration. An HbO decrease prior to the main HbO increase, with its nadir at around 10 s after the burst onset time, was observed in Patients P3 (Fig. 5A purple arrows) and P5 (Fig. 5B pink arrows).

When using the burst period as the comparison baseline, suppression periods were seen to be associated with a large HbO decrease (mean

Fig. 2. Qualitative EEG findings for each neuroICU patient included in the analysis (quantitative EEG, qEEG, results are not shown, but representative qEEG results for each patient is described below). For each patient, a selected EEG clips demonstrating the detected abnormal events is presented. EEG clip legend: In patients identified with non-convulsive seizures, the seizure period was shown with red shadowed blocks; in patients with burst-suppression patterns, green vertical bars indicated the onsets of bursts and red vertical bars indicated offsets of bursts; in patients presenting periodic discharges, the timing of the discharges was marked with yellow vertical bars. Patient P1: qEEG analysis during each seizure revealed bilateral increase in rhythmicity, frequency and amplitude (R > L). Patient P2: qEEG analysis during seizures revealed a bilateral increase (L > R) in rhythmicity, frequency and amplitude. Patient P3: qEEG analysis revealed an increase in rhythmicity, frequency and amplitude during bursts with a strong tendency toward the right hemisphere. Patient P4: qEEG analysis during non-convulsive seizures revealed an increase in rhythmicity, frequency and amplitude (R > L). Patient P5: qEEG analysis during bursts revealed a bilateral increase in rhythmicity, frequency and amplitude. Patient P6: qEEG analysis during seizures (above figure) and bursts (bottom figure) reveal a bilateral increase in rhythmicity, frequency and amplitude. Patient P7: qEEG analysis revealed increases in rhythmicity, frequency and amplitude (R > L) during burst.

Table 2
Summary of electrophysiological and optical findings for each of the seven neuroICU patients.

Patient ID	Events on cEEG			Events on qEEG			Events on fNIRS	
	Main events (number)	Duration (Inter-event-interval)	Localization	Rhythmicity	FFT	Amplitude EEG	Representative HRF	Cortical Areas (HbO changes)*
P1	Burst of spikes/Burst of fast activities (82)	1.5 ± 0.6 s (45.5 ± 58.4 s)	Bi FCT (R > L)	Bi ↑/1–16 Hz	Bi ↑/1–9 Hz (R > L)	Bi ↑ (R > L)	↑ HbO ↑ HbT ↔ ↓ HbR	Bi MFG, SFG
P2	NCSE seizure (102)	24.3 ± 25.9 s (4.6 ± 3.8 s)	Bi FC (L > R)	Bi ↑/1–25 Hz	Bi ↑/1–25 Hz (L > R)	Bi ↑ (L > R)	↑ HbO ↑ HbT ↓ HbR	Bi AntPFC, SFG, PreCG, L STL
P3	BS burst (693)	5.9 ± 8.2 s (2.7 ± 1.3 s)	Generalized	Bi ↑/1–16 Hz	Bi ↑/1–4 Hz (R > L)	Bi ↑ (R > L)	↑ HbO ↑ HbT ↓ HbR	L IFG, TL Bi AntPFC, SFG, MFG, PreCG (diffuse)
	BS suppression (693)	2.7 ± 1.3 s (5.9 ± 8.2 s)	Generalized	Bi ↓	Bi ↓	Bi ↓	↓ HbO ↓↑ HbT ↑ HbR	L IFG, Bi PTL
	LPD (1573)	(1.7 ± 4.3 s)	Bi FCT (R > L)	Bi ↑/1–9 Hz (R > L)	Bi ↑/1–4 Hz (R > L)	Bi ↑ (R > L)	↑ HbO ↑ HbT ↓ HbR	Bi AntPFC, PreCG, MFG, IFG, L TL (diffuse, R > L)
P4	NCSE seizure (64)	10.3 ± 4.4 s (77.1 ± 148.6 s)	Bi CPTO (R > L)	Bi ↑/1–9 Hz	Bi ↑/1–4 Hz (R > L)	Bi ↑	↑ HbO ↑ HbT ↓ HbR	R PreCG, SMG, AntPFC **
	GPD (4649)	(1.2 ± 0.9 s)	Generalized	Bi ↑/1–9 Hz	Bi ↑/1–4 Hz (R > L)	Bi ↑	↓ HbO ↓ HbT ↓ HbR	R PreCG, SMG, AntPFC, IFG, MFG, SFG **
P5	BS burst (206)	55.5 ± 55.9 s (2.2 ± 0.7 s)	Generalized	Bi ↑/1–16 Hz	Bi ↑/1–4 Hz	Bi ↑	↑ HbO ↑ HbT ↓ HbR	Bi AntPFC, IFG, SFG, TL (diffuse)
	BS suppression (205)	2.2 ± 0.7 s (55.5 ± 55.9 s)	Generalized	Bi ↓	Bi ↓	Bi ↓	↓ HbO ↓ HbT ↑ HbR	Bi AntPFC, IFG, SFG, TL (diffuse)
P6	NCSE seizure (33)	5.1 ± 2.3 s (370.7 ± 489.2 s)	Bi FC (L > R)	Bi ↑/1–25 Hz	Bi ↑/1–16 Hz	Bi ↑	↑ HbO ↑ HbT ↓ HbR	L SFG, IFG, R MFG, Bi PreCG, SMG (L > R)
	BS burst (3333)	2.2 ± 1.3 s (2.5 ± 1.6 s)	Generalized	Bi ↑/1–25 Hz	Bi ↑/1–9 Hz	Bi ↑	↑ HbO ↑ HbT ↓ HbR	Bi diffuse FL, L SMG, R PTL
	BS suppression (3330)	2.5 ± 1.6 s (2.2 ± 1.3 s)	Generalized	Bi ↓	Bi ↓	Bi ↓	↓ HbO ↓ HbT ↑ HbR	Bi diffuse FL, L SMG, R PTL
	GPD (1970)	(3.9 ± 3.7 s)	Generalized	Bi ↑/4–16 Hz	Bi ↑/1–16 Hz	Bi ↑	↑ HbO ↑ HbT ↓ HbR	Bi AntPFC, MFG, IFG, SMG, PTL
P7	BS burst (845)	4.6 ± 1.8 s (5.2 ± 2.3 s)	Generalized (R > L)	Bi ↑/1–4 Hz (R > L)	Bi ↑/1–4 Hz (R > L)	Bi ↑ (R > L)	↑ HbO ↑ HbT ↓ HbR	Bi AntPFC, PreCG, R MFG, PTL (R > L)
	BS suppression (844)	5.2 ± 2.3 s (4.6 ± 1.8 s)	Generalized	Bi ↓	Bi ↓	Bi ↓	↓ HbO ↓ HbT ↑ HbR	Bi AntPFC, PreCG, R MFG, PTL

*Approximate locations based on the main HbO response. HbR responses were seen to be more heterogeneous. **Only right hemisphere signal was obtained. Abbreviations. L: left, R: right, Bi: bilateral, FCT: fronto-centro-temporal, FC: fronto-central, CPTO: centro-parieto-temporo-occipital, MFG: middle frontal gyrus, SFG: superior frontal gyrus, AntPFC: anterior prefrontal cortex, PreCG: precentral gyrus, STL: superior temporal lobe, IFG: inferior frontal gyrus, TL: temporal lobe, PTL: posterior temporal lobe, SMG: supramarginal gyrus.

nadir amplitude = 0.019 ± 0.014 μM) and HbR increase (mean PA = -0.050 ± 0.039 μM) in all four patients (Fig. 7), indicating a global reduction in oxygen supply during suppression. Unlike the bursts, the main nadir time of the hemodynamic response to suppression periods seemed to be always around 10 s after the suppression onset regardless of how long the suppression lasted on EEG (with only one exception in Patient 3, bin of 5 s suppression, see Fig. 7A blue arrow).

Cortical projections of the hemodynamic response to bursts confirmed that the increase in HbO and the decrease in HbR were bilateral, and usually affected a large portion of the cortex. However, regions such as the anterior frontal and the central areas were seen to respond more significantly than the others, exhibiting the largest changes in HbO in all of our four patients (e.g., see Fig. 5A–C Cortical projections). Moreover, decreases in HbO were also noticed, especially in the left temporal lobe (e.g., see Patients P3, Fig. 5A, P5, B, P7, D). Short suppression periods (<5s) were associated with a general HbO decrease across the cortex (Fig. 7, bins of suppression<5 s). Interestingly, as suppressions went longer, some hemodynamic "re-activities" were seen, commonly in areas such as temporal and medial prefrontal regions (e.g., see Fig. 7A bin of suppression 5–10 s, Fig. 7C bin of suppression 10–15 s, Fig. 7D bin of suppression 10–15 s).

3.4. Hemodynamic changes associated with PDs

Three patients presented PDs in our cEEG-fNIRS scan. In Patient P3, 1573 right LPDs were identified during bursts of ongoing BS patterns.

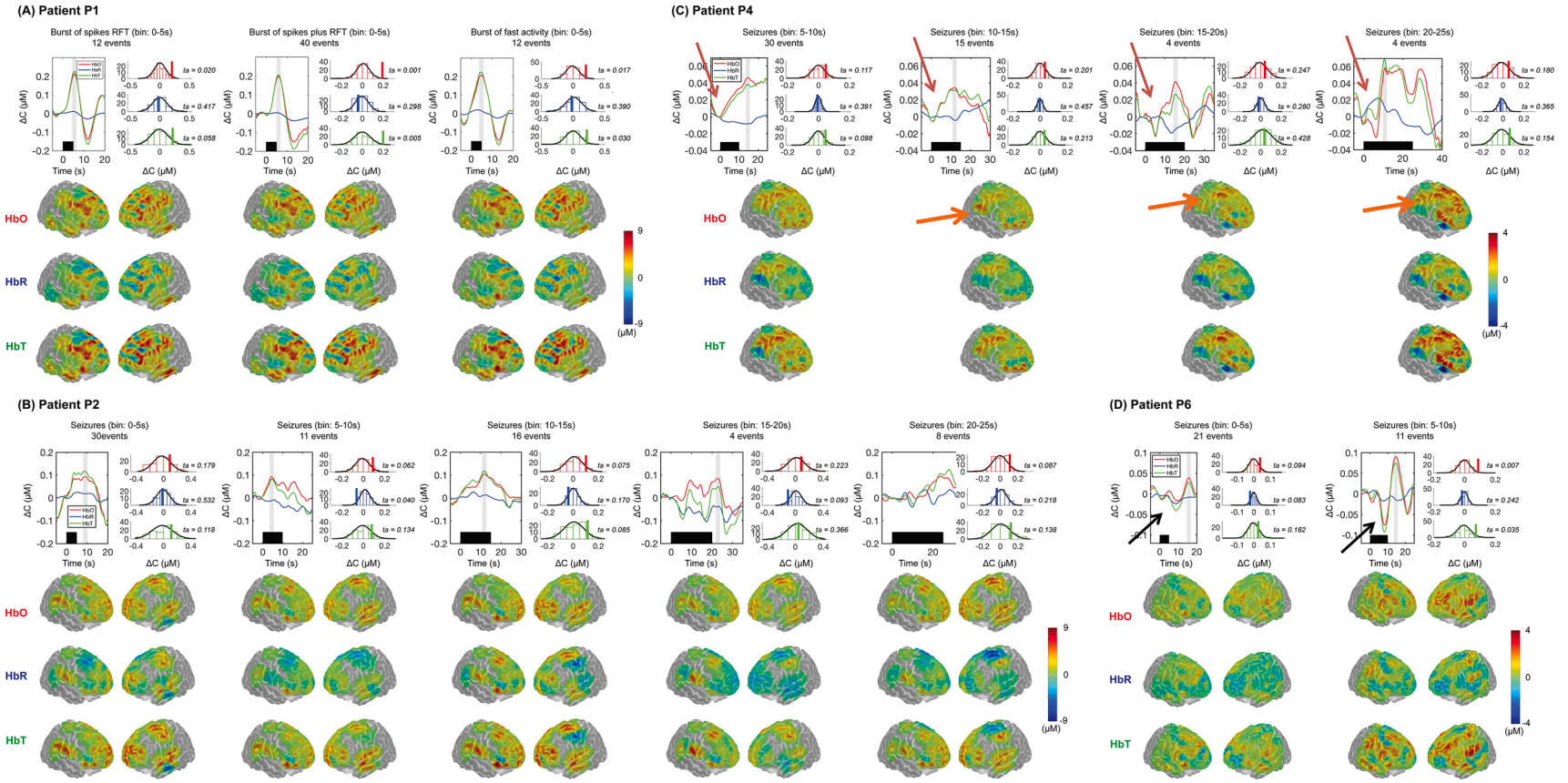

Fig. 3. Hemodynamic changes associated with NCS: (A) Patient P1; (B) Patient P2; (C) Patient P4; (D) Patient P6. Please refer to Fig. S2 for optodes distribution montage and cortical sensitivity profile. The top right panel shows the extracted representative HRFs of HbO, HbR and HbT for each of the seizure bins. Note that no error bar was given as the representative HRF was generated from a PCA analysis of the HRFs of individual channels. Instead, a confidence level represented by the ratio of tail area divided by the PA of the representative HRF relative to the entire distribution area of the amplitudes of spurious HRFs generated from surrogate timecourses was shown. The black horizontal bars indicate the timing of seizures observed on EEG. The bottom right panel depicts the cortical projections of PA (averaged within a 2-sec window around the maximum value, or the minimum value if a nadir was detected). The PA time periods averaged are also highlighted with gray shaded bars directly on the representative HRF plots. For Patient P4, only the right-side projections are shown, as cortical coverage was limited on the left side due to the patient's position during the scan.

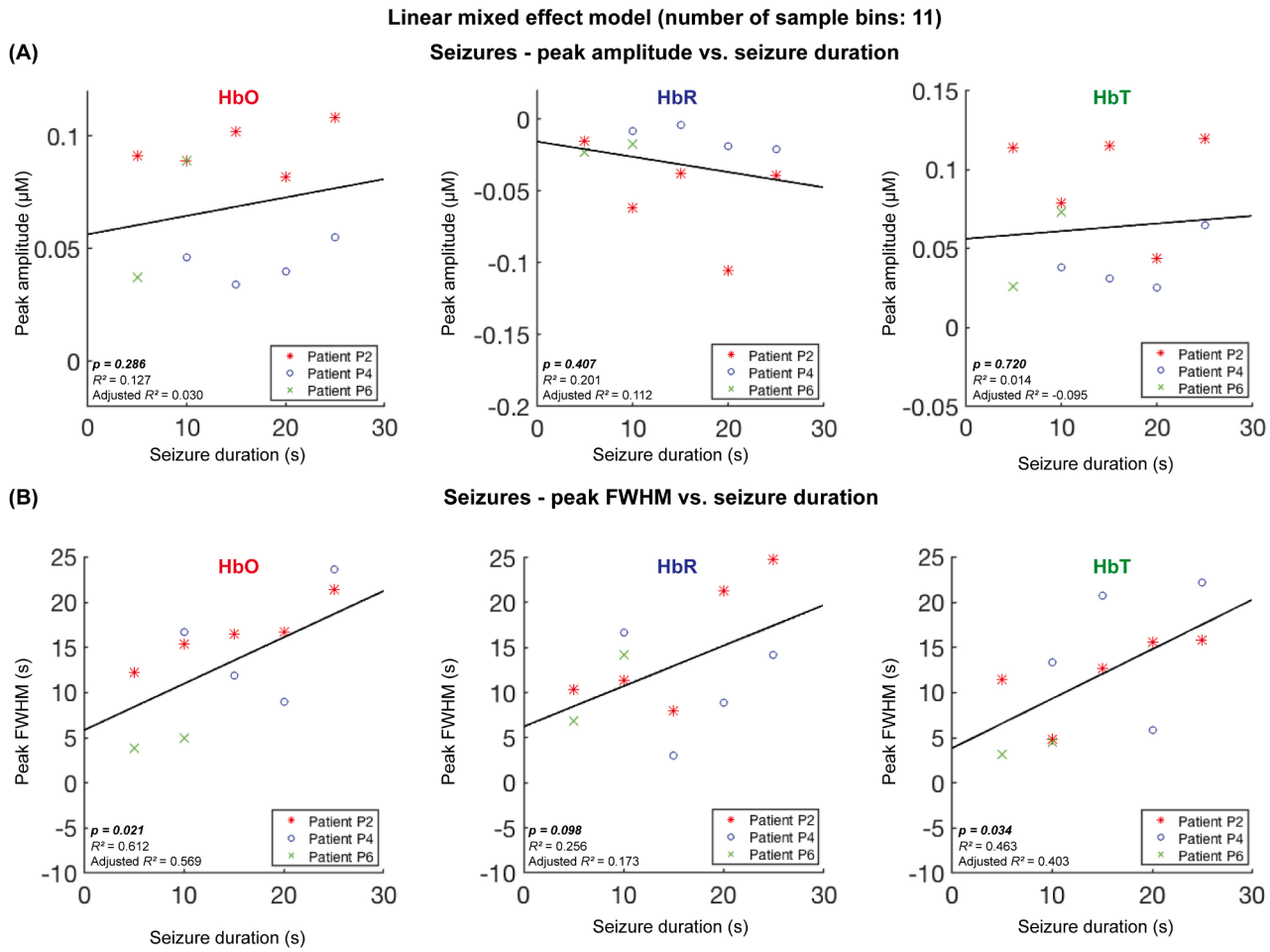

Fig. 4. Regression plots of linear mixed effect regression models relating (A) PA and (B) peak FWHM of representative HRFs to seizures to the duration of seizures identified on EEG. Statistically significant results were obtained for HbO Peak FWHM vs. Seizure duration ($p = 0.021$) and HbT Peak FWHM vs. Seizure duration ($p = 0.034$). The black lines depicted the predicted values using only the fixed effect regression coefficients for demonstration purposes.

For Patient P4, we identified 4649 GPDs, including 363 GPDs occurring during NCS (denoted as "ictal PDs"), and 4286 GPDs during interictal periods (i.e. "interictal PDs"). Patient P6 presented patterns of NCSE, continued BS and GPDs throughout the recording. The detected 1970 GPDs only occurred during interictal bursts and not during seizures.

The representative HRFs to PDs showed hemodynamic response with an expected shape in Patients P3 (Fig. 8A) and P6 (Fig. 8C), characterized by a major increase in HbO (mean PA = 0.012 μM) and HbT (mean PA = 0.011 μM) as well as a decrease in HbR (mean nadir amplitude = -0.004 μM), followed by an undershoot. The peaking time of HbO **response** was around 1.6 s and 3.8 s for Patient P3 and P6 respectively, which was earlier than that seen in adult canonical HRFs (peaking around 5–6 s). The representative HRF to PDs showed an inverted shape in Patient P4 with a notable decrease in HbO (PA = -0.007 μM) and in HbT (PA = -0.007 μM) for ictal PDs (Fig. 8B). These decreases were much less significant with interictal PDs, showing a lower nadir amplitude (-0.002 μM for HbO and HbT) and a lower nadir FWHM, e.g., 3.5 s for HbO compared with 8.6 s associated with ictal PDs.

Cortical projection of hemoglobin concentration changes showed bilateral and widespread HbO and HbR responses in Patients P3 (Fig. 8A) and P6 (Fig. 8C). Furthermore, in those two patients, the cortical areas that exhibited the strongest changes were seen to highly overlap the regions responding to bursts or seizures in the previous analysis (e.g., for Patient P3, see Fig. 5A Cortical Projections of Burst bins 15–20 s and 20–25 s). For Patient P3, we observed more significant HbO increase (with regards to response magnitude) in the right side relative to the left side (Fig. 8A), which was concordant with the EEG finding of LPDs lateralized to the right hemisphere. For Patient P4, simultaneous decreases in HbO and HbR were identified in the frontal regions. However, the central areas showed distinct responses to GPDs, with an HbO decrease following ictal GPDs but a more canonical HbO increase following interictal PDs (see the projected regions marked with black arrows in Fig. 8B).

3.5. Case studies

Below, we provide two case studies to illustrate our study procedures and results in details.

3.5.1. Illustrative case 1, patient P3

A 52-year-old woman with right frontal lobe glioblastoma multiforme (partially resected and treated with radiation four years prior) was admitted for clinical seizures followed by NCSE successfully treated with antiseizure medications and anesthetics towards a burst-suppression pattern. Brain CT showed mild right frontal vasogenic edema (Fig. S2C, right). cEEG-fNIRS monitoring was conducted for a total of 4.5 h, from which 100 min of recording were selected for analysis. During that time period, she presented 693 episodes of burst and suppression (average duration: 5.9 ± 8.1 s, average frequency: 0.1 Hz) and 1573 right frontal LPDs spreading to the left frontal region (average frequency: 0.6 Hz). While BS patterns were generalized, they were observed to be more predominant over the left hemisphere (Fig. 2C).

Fifty-five valid fNIRS channels covered the bilateral anterior

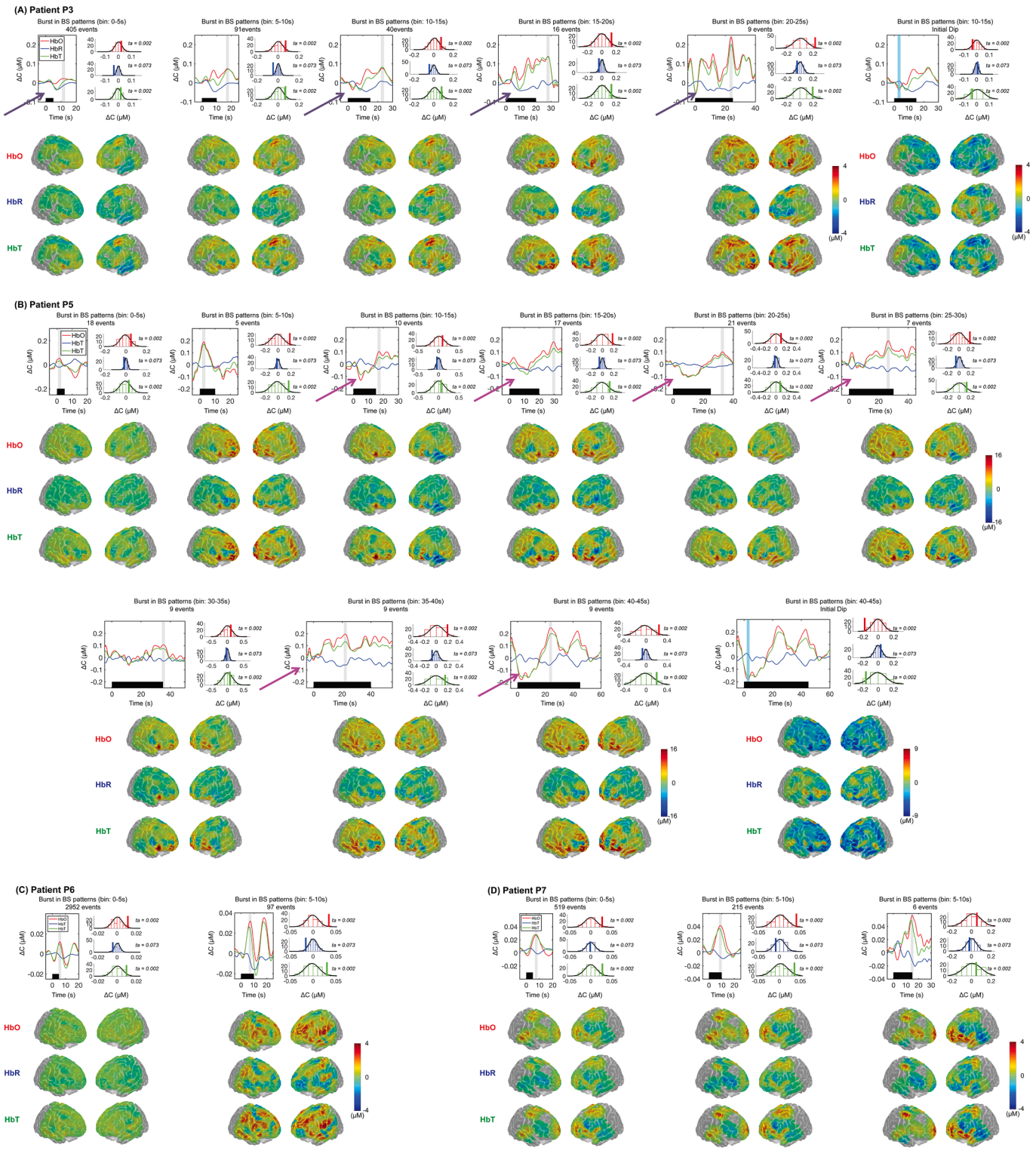

Fig. 5. Hemodynamic changes associated with BS bursts: (A) Patient P3; (B) Patient P5; (C) Patient P6; (D) Patient P7. Please refer to Fig. S2 for optodes distribution montage and cortical sensitivity profile. The top right panel shows the extracted representative HRFs of HbO, HbR and HbT for each of the burst bins. A confidence level represented by the ratio of tail area divided by the PA of the representative HRF relative to the entire distribution area of the amplitudes of spurious HRFs generated from surrogate timecourses was shown for each representative HRF. The black horizontal bars indicate the timing of bursts observed on EEG. The bottom right panel depicts the cortical projections of PA. The PA time periods averaged are also highlighted with gray shaded bars directly on the representative HRF plots. For Patient P3 and P5, the last set of projections showed the spatial profile of hemodynamic changes around the initial HbO "dipping" period (highlighted in cyan on the HRF plots).

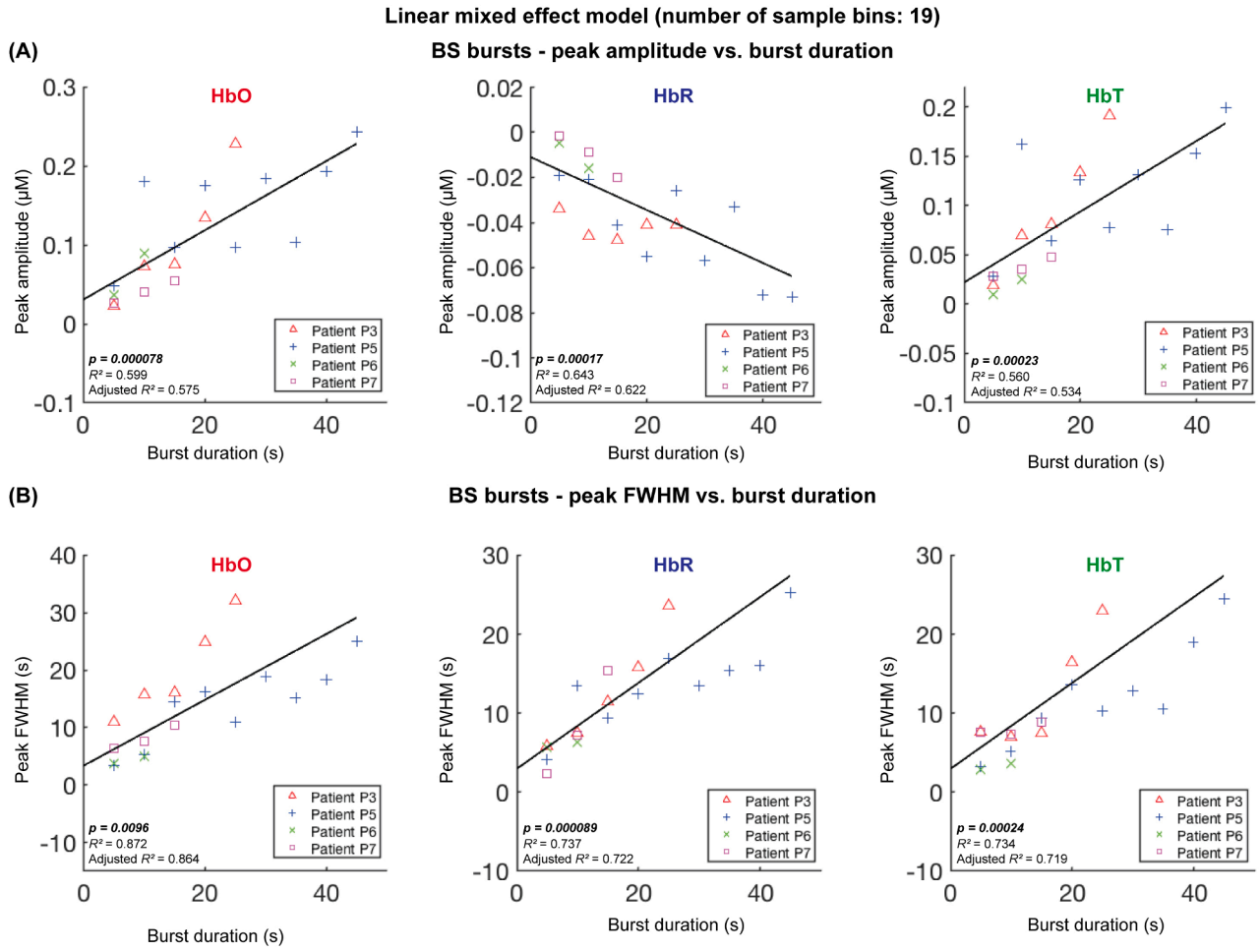

Fig. 6. Regression plots of linear mixed effect regression models relating (A) PA and (B) peak FWHM of representative HRFs to BS bursts to the duration of bursts identified on EEG. Statistically significant results were obtained for HbO PA vs. Burst Duration ($p = 0.000078$), HbR PA vs. Burst Duration ($p = 0.00017$), HbT PA vs Burst Duration ($p = 0.00023$), HbO FWHM vs. Burst Duration ($p = 0.0096$), HbR FWHM vs. Burst Duration ($p = 0.000089$), and HbT FWHM vs. Burst Duration ($p = 0.00024$). The black lines depicted the predicted values using only the fixed effect regression coefficients.

prefrontal cortex, medial prefrontal and central regions, and part of the temporal regions (Fig. S2C, left). In the bin analysis, the 693 bursts were grouped into 12 bins. Fig. 5A depicts the representative HRFs to bursts for bins from [0 to 5 s] to [20 s to 25 s], which contained a total of 670 bursts (≈ 97%). These HRFs of the five bins showed that, relative to the suppression periods, bursts were generally associated with an increase in HbO and HbT as well as a decrease in HbR. Moreover, the durations of the hemodynamic responses were seen to be longer and the magnitudes of the main peak were larger for bursts that lasted longer (Fig. 5A). Early decreases, or reductions in the increases for some bins, of HbO and HbT were also observed, which reached the nadir at around 10 s after the onset of the bursts. However, such "inverted" changes were not observed for HbR. For this patient, cortical projections revealed inhomogeneous pattern of hemoglobin concentration changes in different parts of the brain (Fig. 5A Cortical Projections). With shorter bursts, the area with the highest level of responsivity was seen to be within the left inferior frontal gyrus. With longer bursts, the increases in HbO were found to be larger across the fNIRS-covered cortex. Consistent with EEG findings, the amplitude of the response was larger for channels located in the left hemisphere than those in the right hemisphere. For example, for the bin of bursts between 20 s and 25 s, the mean PA of HbO response (averaged across a 2-sec window centered at 23.85 s) was 0.232 μM for left hemisphere channels and 0.216 μM for right hemisphere channels. The HRF analysis of suppression periods relative to bursts showed a decrease in HbO and an increase in HbR for both the [0 to 5 s] bin (containing 541 suppression periods) and the [5 s to 10 s] bin (27 suppression periods). Unlike the bursts, longer suppression periods (>5 s) seemed to elicit a much higher HbR increase but an overall weaker HbO decrease for this patient (Fig. 7A). Consistent with the representative HRFs, cortical projection maps revealed several brain regions that elicited a HbO increase with long suppression periods (while short suppression was associated with a more or less global HbO decrease), including the left anterior temporal lobe and the bilateral precentral areas (Fig. 7A Cortical Projections). These results suggested that, despite continued suppression of neuronal activity, rapid changes in the level of oxygen consumption blood supply might still take place in some brain regions towards the end of long suppression periods.

Due to the briefness of the LPDs, the 1519 right frontotemporal LPDs were grouped into a single bin of [0 to 5 s]. These LPDs were present only within the bursts, with an overall mean IPDI of 1.7 s (frequency = 0.6 Hz). The representative HRFs showed an expected increase in HbO and HbT as well as a decrease in HbR following the LPDs (Fig. 8A). The HbO and HbT increases were seen to peak at around 1.6 s, followed by an undershoot with its nadir at around 9.45 s after the LPD. The decrease in HbR reached the minimum value 2.6 s after the HbO peak, at around 4.2 s post-LPD. Cortical projections revealed bilateral HbO increases in most of the cortical areas covered by fNIRS, showing widespread hemodynamic response to LPDs (Fig. 8A Cortical Projections). The mean HbO PA across channels was seen to be larger in the right hemisphere (0.013 μM) than in the left hemisphere (0.011 μM). These observations

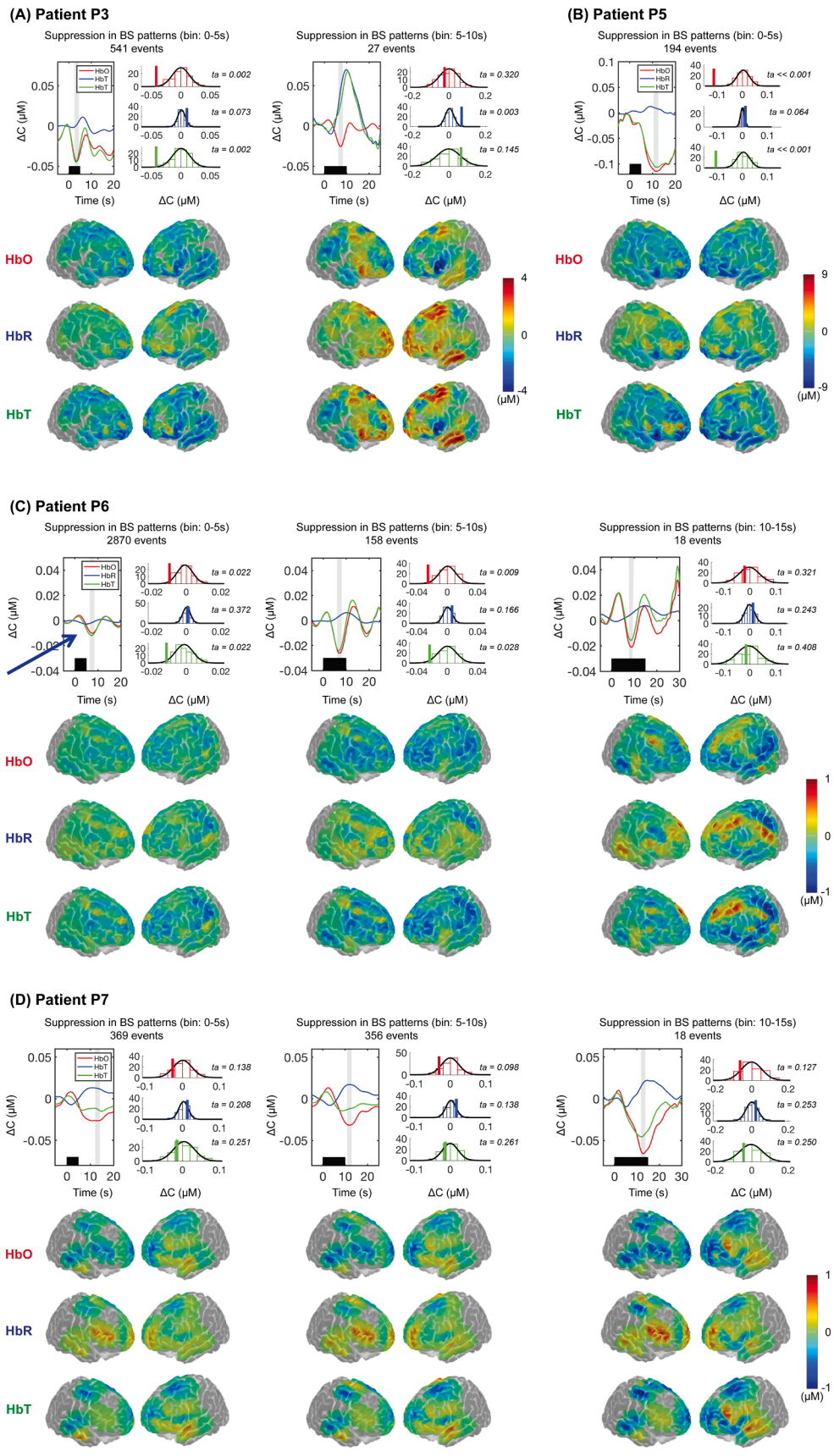

Fig. 7. Hemodynamic changes associated with BS suppressions: (A) Patient P3; (B) Patient P5; (C) Patient P6; (D) Patient P7. Please refer to Fig. S2 for optodes distribution montage and cortical sensitivity profile. The top panel shows the extracted representative HRFs of HbO, HbR and HbT for each of the suppression bins. A confidence level represented by the ratio of tail area divided by the PA of the representative HRF relative to the entire distribution area of the amplitudes of spurious HRFs generated from surrogate timecourses was shown for each representative HRF. The black horizontal bars indicate the timing of suppression observed on EEG. The bottom panel depicts the cortical projections of PA. The PA time periods averaged are also highlighted with gray shaded bars directly on the representative HRF plots.

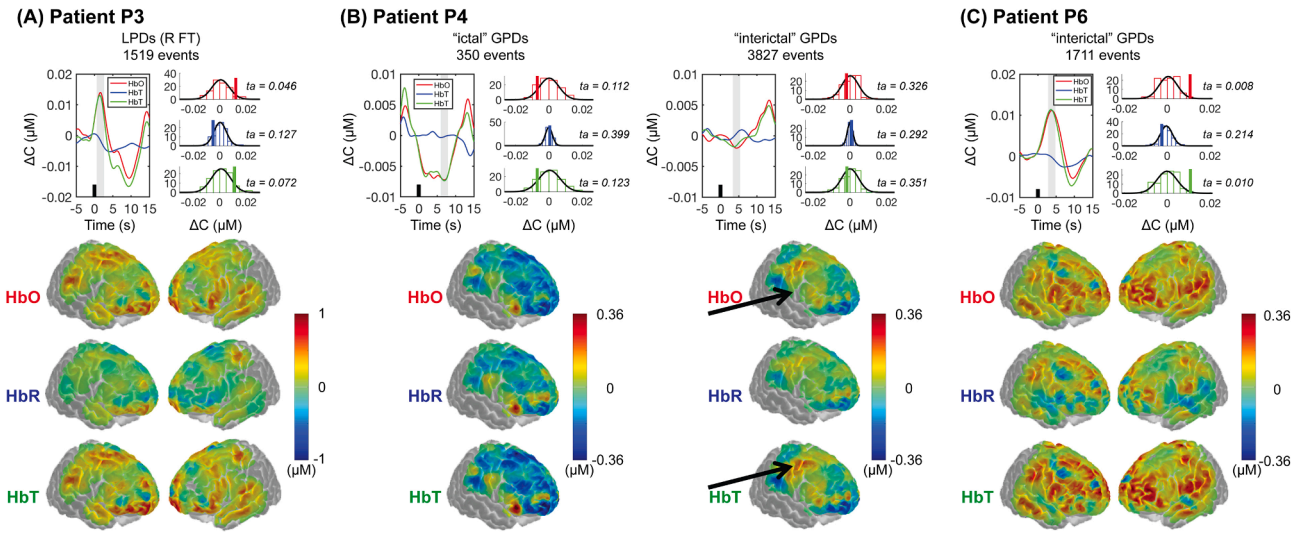

Fig. 8. Hemodynamic changes associated with PDs: (A) Patient P3; (B) Patient P4; (C) Patient P6; (D) Patient P7. Please refer to Fig. S2 for optodes distribution montage and cortical sensitivity profile. The top panel shows the extracted representative HRFs of HbO, HbR and HbT for PD bins. A confidence level represented by the ratio of tail area divided by the PA of the representative HRF relative to the entire distribution area of the amplitudes of spurious HRFs generated from surrogate timecourses was shown for each representative HRF. The black vertical bars indicate the timing of PDs observed on EEG. The bottom panel depicts the cortical projections of PA. The PA time periods averaged are also highlighted with gray shaded bars directly on the representative HRF plots. For Patient P4, note that the highlighted window for "interictal" GPDs was selected to be around 4.4 s (minimum value of the initial HbO decrease) instead of 13.35 s. The main HbO response of "interictal" GPDs, similar to that of "ictal" GPDs, was identified to be the first nadir. The HbO increase peaking at 13 s was likely part of the overshoot following the initial HbO decrease.

potentially implied a retained neurovascular coupling process for the generation of LPDs in this patient, albeit of a shorter hemodynamic response time.

3.5.2. *Illustrative case 2, patient P4*

A 57-year-old male patient with hepatic cirrhosis was admitted to the neuroICU for gastrointestinal bleeding, melena and metabolic encephalopathy. On admission day 1 the patient presented myoclonus, which later evolved, from day 2 and 3 to generalized tonico-clonic seizures, convulsive SE and eventually NCSE on day 4. Two sessions of cEEG-fNIRS was performed 7 days after admission (total duration: 7 h), of which a period of 97 min was selected for analysis. MRI revealed T2/FLAIR hypersignal and restriction diffusion bilaterally in parietal, temporal, insular and cingulate, and thalami regions (Fig. S2D, right). Sixty-four bilateral seizures (maximum over the right centro-parieto-temporo-occipital regions) with an average duration of 10.3 ± 4.4 s and an averaged interictal period of 77.1 ± 148.6 s, as well as 4649 GPDs (mean IPDI = 1.2 s and mean frequency = 0.8 Hz) were identified from the EEG data (Fig. 2D).

Forty-one valid fNIRS channels were distributed over the bilateral anterior prefrontal cortex, the right medial prefrontal cortex and the right precentral areas (Fig. S2D, left). Unfortunately, due to the patient's position during the scan, fNIRS channels covering the left medial prefrontal and central areas yielded a low SNR and had to be excluded. Based on their durations, 53 NCS were grouped into four different bins with ranges from [5 s to 10 s] to [20 s to 25 s], for which the representative HRFs are shown in Fig. 3C. From the HRFs, we identified an increase in HbO and HbT, and a decrease in HbR (relative to the interictal period) that were associated with the seizures in all of the four bins. Similar to the bursts observed in the previous case study, seizures with longer durations seemed to elicit hemodynamic responses that were also longer in duration and higher in peak magnitude. The initial decrease in HbO and HbT and the increase in HbR prior to the main response (i.e. the "initial dip") were also noticed, especially for seizures that lasted longer. Cortical projections of the concentration changes in the right hemisphere highlighted distinct regions that showed the largest HbO response magnitude within the right central and the right frontocentral areas (Fig. 3C Cortical Projections, Orange arrows).

Among the 4177 included GPDs, 3827 GPDs were recorded during the interictal periods (denoted as the "interictal GPDs" in this section) while the rest 350 GPDs were captured during seizures (denoted as the "ictal GPDs"). These two types of GPDs were treated as separate conditions in our HRF analysis to further explore the potential differences in the mechanism. Unlike the other two patients who also presented PDs (Patients F3 and F6), the representative HRFs to the ictal GPDs in this patient were characterized mainly by a large decrease in HbO and HbT along with a small decrease in HbR concentration (Fig. 8B). The HbO decrease reached its nadir at around 6.95 s after the GPD onset. Cortical projection of the HbO concentration revealed that the negative response was seen over a large portion of the covered right hemisphere, including the right anterior prefrontal, the medial prefrontal and the central areas (Fig. 8B Cortical Projections). On the other hand, representative HRFs to interictal GPDs showed overall much lower HbO and HbT decreases, while the HbR level stayed almost unchanged. In fact, interictal GPDs were observed to elicit a similar HbO decrease in the right anterior prefrontal cortex. However, in the right central area where the large magnitude of hemodynamic response to seizures was located in the previous NCSE analysis, we observed an HbO increase and an HbT increase following interictal GPDs with an expected shape (Fig. 8B black arrows). These results suggested that the neurovascular coupling for GPDs might be disrupted in some cases. For this particular patient, potential risk factors included the co-presence of seizures and a higher PD frequency (0.8 Hz as opposed to 0.6 Hz in Patient F3 and 0.3 Hz in Patient F6). The hemodynamic response with an expected shape, i.e. increases in HbO and decreases in HbR, to interictal GPDs in the right central area indicated less stress on local oxygen supply for GPDs when seizure activities were not continued.

4. Discussion

To the best of our knowledge, this study is the first to report simultaneous electrophysiological and hemodynamic changes observed in critically ill adults patients presenting with SE, PDs and pharmacologically induced BS patterns using cEEG-fNIRS. Through the analysis of

seven patients, we assessed the feasibility and the clinical value of cEEG-fNIRS for long-term monitoring in the neuroICU.

4.1. Increased blood oxygenation during seizures in status epilepticus

SE represents an extreme ictal phenomenon, in which "normal" mechanisms responsible for seizure termination fail. Among those mechanisms, hypoxia has been proposed (Zubler et al., 2014). Animal models of SE generally showed an increase in cortical blood oxygenation due to higher metabolism of the ictal state (Lee et al., 2018). In humans, both states of hyper and hypometabolism have been reported in patient with NCSE (Siclari et al., 2013). For example, EEG-fMRI acquisition in focal motor status epilepticus cases (*epilepsia partialis continua*) shows a BOLD signal increase in the focus combined with a widespread BOLD signal deactivation (Lazeyras et al., 2000). This dynamic reflects the redistribution of CBF and extreme focal modulation of oxygen extraction in the benefit of the hyperactive ictal focus. Indeed, despite the increase in CBF, anaerobic metabolic distress (increase in lactate/pyruvate ratio) and glutamate excitotoxity have been documented during focal NCSE in patients with TBI (Vespa et al., 2007). Our findings are in line with previous studies in which ictal metabolism level during SE is associated with an increase in CBF and brain oxygenation. In all three patients, an increase in HbO, generally of larger amplitude, and a decrease in HbR, generally of lower amplitude were observed during seizures. These changes most likely suggested an increase in CBF and CBV that over-compensated the ictal increase in neuronal oxygen needed. In addition, these changes were proportional to seizure duration with shorter seizures manifesting with lower relative HbO increase and HbR decrease, showing potentially sufficient oxygen supply even towards the end of the seizures. Overall, our data do not seem to support the hypothesis that hypoxia is the main cause of seizure termination in SE.

Another important finding is that the fNIRS-measured hemodynamic responses were generally the largest in the focal cortical areas involved in seizures. This is clinically important as fNIRS have the potential to not only help in the diagnosis of NCS and NCSE, but also in improving seizure localization.

4.2. Non-uniform cortical hemodynamic profile during burst-suppression

The traditional perception of BS, as a uniform and global state of brain activity, has been challenged over the last decade (Ferron et al., 2009; Lewis et al., 2013). In vivo studies in the anesthetized cat have shown that neuronal activity in subcortical structures can be increased during suppression, which may elicit bursts sequences in the hyperexcitable cortex (Amzica, 2009). More recently, intracranial EEG recordings performed in anesthetized patients undergoing epilepsy surgery revealed the asynchronous nature of burst-suppression patterns across the cortex (i.e. burst and suppression not occurring at the exact same time and in all regions alike) (Lewis et al., 2013). Neurovascular dynamics and cerebral metabolism seem to be among critical processes underlying the genesis of BS patterns (Ching et al., 2012; Lewis et al., 2013). Using fMRI, spontaneous multifocal fluctuation in CBF and BOLD signals during BS has been observed in anesthetized swine and rats (Liu et al., 2011; MÄkiranta et al., 2002). Optical imaging (NIRS and diffuse correlation spectroscopy) with simultaneous scalp-EEG have also been used in anesthetized rats and showed an increase in metabolism and CBF associated with each burst (Sutin et al., 2014). In humans, transient stereotypic changes characterized by an initial HbO decrease followed by a pronounced HbO increase during spontaneous bursts was reported in premature neonates presenting with neurological distress (Roche-Labarbe et al., 2007), and during hypothermia-induced BS in infants with hypoxic-ischemic encephalopathy (Chalia et al., 2016). The shape of the response was seen to be highly variable across different brain regions and different patients.

This pilot study is the first to assess hemodynamic features of BS in comatose adults. Our results were largely consistent with these previous reports, showing an overall but spatially inhomogeneous increase in HbO and a less significant overall decrease in HbR during bursts relative to the suppression period in all of the four patients in whom BS patterns were identified. The relationship between the amplitude and the duration of the HbO increase and burst length seen on EEG suggested that the neuronal metabolism was adequately compensated. The initial decrease in HbO as noted in previous studies (Chalia et al., 2016; Roche-Labarbe et al., 2007), or an initial reduction in HbO increase, was also noticed in most of our patients. On the other hand, short suppression periods were followed by a more global (but also spatially inhomogeneous) reduction in HbO, suggesting an acute drop in neuronal activity and oxygen supply. Interestingly, the spatial profile of the HbO decrease in the HRF to suppression periods was seen to highly overlap with the spatial profile of the initial HbO decrease in the HRF to bursts (e.g., see the similarity between the spatial profiles of projected hemoglobin concentration changes between Fig. 5A Projection of initial dip and Fig. 7A bin of 0–5 s, as well as between Fig. 5B Projection of initial dip and Fig. 7B). This suggest that the initial HbO decrease seen in the response to bursts, which usually reached its nadir at around 5–10 sec after the burst onset, could possibly be part of a delayed hemodynamic effect of the suppression periods preceding the bursts. An alternative interpretation is that the initial mismatch between oxygen demand and blood supply at the beginning of bursts occurs at cortical sites that have been mostly suppressed in the suppression periods. Nevertheless, our results provide further evidence for non-uniform hemodynamic changes during BS patterns, and highlight the potential of using fNIRS to study the spatial distribution of this response.

4.3. Potential factors associated with hemodynamic response to PDs

Clinical management of critically ill patients presenting with EEG patterns falling within the IIC still poses a significant challenge to physicians. In addition to considering clinical factors (e.g., response to treatment), researchers have resorted to multimodal neuroimaging techniques to better understand the "ictal vs. interictal nature" of these patterns, their impact on the brain and improve the management of the critically ill presenting with IIC patterns (Claassen, 2009). Both FDG-PET hypermetabolism and hypometabolism have been observed in patients with PDs patterns (Sakakibara et al., 2014; Struck et al., 2016). In another study by Vespa et al., PDs displayed a metabolic crisis similar to what has been previously seen during seizures by the same authors (Vespa et al., 2016). More recently, Witsch et al. used invasive EEG recordings, brain tissue oxygen tension (PbTO2), and rCBF in patients presenting with subarachnoid haemorrhage (SAH) (Witsch et al., 2017). In their study, PDs (GPDs and LPDs) > 2 Hz were associated with a decrease in PbTO2, while an increase in PbTO2 was observed for $0.5 <$ PDs < 2 Hz. Based on these observations, the authors suggested a metabolic decompensation was most likely to occur when PDs > 2 Hz, and, therefore, would require more aggressive treatment.

In our study, two of the three patients with PDs presented an overall increase in HbO and HbT as well as a decrease in HbR (one with GPD and one with LPD), potentially suggesting a normal neurovascular coupling process and sufficient compensation of oxygen following the PDs. These findings are in line with the features reported by Witsch et al. (Witsch et al., 2017) in PDs ≤ 2 Hz. The hemodynamic mapping of these changes was widely spread in patients with GPDs, and more focalized in LPDs. However, in the other patient (Patient P4), we observed an inverted shape of HbO and HbT responses to GPDs. This might be due to a higher PD frequency detected in the patient (0.8 Hz compared with 0.6 Hz in Patient P3 and 0.3 Hz in Patient P6) or the co-presence of seizures. In particular, the GPDs occurring during the seizures (ictal GPDs) showed a prominent HbO decrease over a large portion of the right hemisphere, while the GPDs within the interictal periods were associated with similar HbO decreases in the prefrontal cortex but a weak HbO increase around the presumed epileptic focus area. These observations implied a possible change CBF and blood oxygenation from the other portion of the cortex

towards the focus area during PDs. Moreover, the hemisphere-wise HbO and HbT decrease following ictal PDs revealed inadequate oxygen reserve for PDs during seizures, leading to a potential hypoxic-ischemic state. While further confirmation of our results is needed, these data showcase the advantages of cEEG-fNIRS in delineating the full dynamic profile of the hemodynamic response associated with PDs and its potential to be used to assist in the process of clinical management.

4.4. Feasibility of conducting cEEG-fNIRS in the neuroICU

The current work represents the first study of using combined cEEG-fNIRS in the adult neuroICU to monitor hemodynamic changes associated with abnormal EEG events, including SE, medically-induced BS and PDs. We were able to place a large number of fNIRS optodes (>50) to enable coverage of nearly the full head (except occipital and posterior temporal/parietal areas), and performed long-term EEG-fNIRS recordings in 11 comatose patients (for up to 32 h). These progresses are important in showing the feasibility of conducting continuous hemodynamic monitoring in the neuroICU. The results revealed specific and dynamic patterns associated with brief and ongoing EEG events over a long period of time. However, special arrangements in both the data acquisition and analysis had to be made to accommodate the complex data collection environment of the neuroICU. While the patients are comatose, their bodies are normally kept in a supine position and their heads tilted towards a certain direction by a pillow. This can complicate the process of installing optodes and maintaining good skin contact in the back and left posterior side of the head. In addition, the presence of stitches, invasive probes and edema may also complicate optode installation. The continuity of fNIRS measurements can be affected by routine clinical care (e.g., examination, blood sampling, suctioning, clapping), imaging needs (e.g., CT, MRI), and some forms of medical interventions (e.g., bronchoscopy). Moreover, examination and care provided by the medical staff and nurses, as well as the use of low air loss beds in the critically ill, for pressure wounds prevention, can affect the quality of fNIRS measurement by creating significant motion artifacts during the monitoring. In our pilot study, many fNIRS channels had to be excluded due to loss of contact, low SNR or excessive motion artifacts. The exclusion of channels led to reduced coverage of brain areas and inhomogeneous sensitivity in cortical detection, which limited our ability in delineating the spatial features of the hemodynamic responses. One possible way to reduce motion artifacts and prevent optode from sliding during the monitoring would be to glue optodes with collodion (Yücel et al., 2014) directly on the scalp in the same way EEG electrodes are glued for long-term monitoring in epilepsy units. Finally, performing long-term continuous cEEG-fNIRS recording provides huge amount of recorded data. Rather than the offline GLM analysis employed in this study, clinical monitoring using cEEG-fNIRS will almost certainly require online data processing. Recent advances in real-time analysis methods such as those developed for brain-computer interfaces (Lührs and Goebel, 2017) may be considered for a faster feedback of the patient's brain electrophysiological and hemodynamic condition. Nevertheless, the review of EEG/fNIRS data, the identification of abnormal EEG events of interest and their alignment under an offline GLM or online data processing may pose significant practical challenges.

4.5. Limitations

This study has several limitations. First is the small sample size for each type of EEG patterns (despite a larger number of patients compared to previous studies). The results presented in this paper mostly involve short-duration events e.g., <25 s for SE seizures and <35 s for bursts in BS patterns. Our findings will have to be validated in a larger cohort of patients. Second, substantial heterogeneity (e.g., regarding age, sex, anatomical differences, type of brain injury, co-morbidities, treatment) exist in our population, which can potentially impact brain hemodynamic signals. Third, systemic physiological factors can also affect cerebral blood flow (Rostrup et al., 2002). While we used clinical records of different systemic physiological measurements to "grossly" exclude periods characterized by abnormal or fluctuating vital signs, it was not possible to use these measurements as covariates in our analysis due to their low temporal resolution. Fourth, short-distance optodes were not used to quantify and subtract the contribution of superficial layers (e.g., scalp, skin and skull) to the fNIRS signal. While there are currently no guidelines or gold standard for removing physiological contamination from the fNIRS signal, we decided in this study to use a PCA filter removing 90% of the global variance. However, some residuals may remain. Finally, while our previous studies revealed significant nonlinear suppression effect in the hemodynamic response to epileptic events that might happen in rapid succession (Peng et al., 2016; Pouliot et al., 2012) (which was the case in many of our patients included in this study, e.g., patients who had PDs with a high frequency), nonlinearity was not specifically modeled in the GLM for the sake of model simplicity and data processing time. The neglect of the nonlinear component in the model may partially account for the relatively low amplitudes of representative HRFs seen in this study compared with previous work (e.g., see Fig. 8 where the amplitudes of HRF to PDs were of the order of 0.01 μM). Other factors that may affect the representative HRF amplitudes include the averaging of HRFs across all channels instead of targeting at a particular activated region, the empirical choice of the partial pathlength factor, the relatively low low-pass filter cutoff frequency (0.2 Hz), and the loss of elasticity of cortical tissue in eliciting hemodynamic responses after repetitive, excessive neuronal firing (Arango-Lievano et al., 2018). Future studies further delineating the effects of these physiological or analytical factors may be needed to develop an analysis method that is a more suitable for this type of long and complex neuroICU data.

5. Conclusions

In conclusion, we conducted long-term cEEG-fNIRS recordings in the neuroICU, and analyzed the hemodynamic response to abnormal EEG patterns identified from seven comatose patients. In most cases, the electrical activity in seizures, bursts and PDs was associated with an overall increase in HbO and a decrease in HbR, with the amplitudes and durations of the hemodynamic changes positively correlated to the EEG length of the events. These responses were seen to be spatially inhomogeneous and specific to patients. Our results suggested that normal neurovascular coupling might be partially retained during these abnormal EEG patterns, while highlighting the highly varying nature of these changes across conditions and patients. This pilot work shows the feasibility of conducting cEEG-fNIRS in the neuroICU, however more extensive studies with a larger patient cohort and more advanced data collection and analysis methods (e.g., to further enlarge cortical coverage, reduce motion artifacts, and establish real-time online assessment of cortical responses) are needed to straighten our conclusions, as well as to encourage clinical hemodynamic and electrophysiological monitoring which may help rethink strategies for patient care and treatment in the neuroICU.

CRediT authorship contribution statement

Ali Kassab: Software, Validation, Formal analysis, Investigation, Data curation, Writing – original draft, Writing – review & editing, Visualization. **Dènahin Hinnoutondji Toffa:** Formal analysis. **Manon Robert:** Resources. **Frédéric Lesage:** Methodology, Writing – review & editing, Supervision, Project administration, Funding acquisition. **Ke Peng:** Methodology, Software, Validation, Formal analysis, Writing – original draft, Writing – review & editing, Visualization. **Dang Khoa Nguyen:** Conceptualization, Methodology, Writing – review & editing, Supervision, Project administration, Funding acquisition.

Declaration of Competing Interest

The authors declare that they have no known competing financial interests or personal relationships that could have appeared to influence the work reported in this paper.

Acknowledgements

We thank all study subjects and family for their valuable participation. We also thank the ICU nurses and physicians for their support and patience during our study.

This work was supported by the Canadian Institutes of Health Research (CIHR) (MOP 133643), the National Sciences and Engineering Research Council in partnership with CIHR (CPG-127774), the Canada Research Chair Program (DKN and FL), the Fonds de recherche du Québec – Santé (AK) and the TransMedTech Excellence Scholarship from Canada First Research Fund (KP). The datasets generated during and/or analyzed during the current study are available from the primary or corresponding author on reasonable request.

Appendix A. Supplementary data

Supplementary data to this article can be found online at https://doi.org/10.1016/j.nicl.2021.102880.

References

Aasted, C.M., Yücel, M.A., Cooper, R.J., Dubb, J., Tsuzuki, D., Becerra, L., Petkov, M.P., Borsook, D., Dan, I., Boas, D.A., 2015. Anatomical guidance for functional near-infrared spectroscopy: atlasviewer tutorial. Neurophotonics 2 (2), 020801. https://doi.org/10.1117/1.NPh.2.2.020801.

Amzica, F., 2009. Basic physiology of burst-suppression. Epilepsia. https://doi.org/10.1111/j.1528-1167.2009.02345.x.

Arango-Lievano, M., Boussadia, B., De Terdonck, L.D.T., Gault, C., Fontanaud, P., Lafont, C., Mollard, P., Marchi, N., Jeanneteau, F., 2018. Topographic reorganization of cerebrovascular mural cells under seizure conditions. Cell Rep. 23 (4), 1045–1059. https://doi.org/10.1016/j.celrep.2018.03.110.

Bansal, L., Miller, I., Hyslop, A., Bhatia, S., Duchowny, M., Jayakar, P., 2016. PET hypermetabolism in medically resistant childhood epilepsy: Incidence, associations, and surgical outcome. Epilepsia 57 (3), 436–444. https://doi.org/10.1111/epi.13311.

Berndt, N., Kovács, R., Schoknecht, K., Liotta, A., n.d. Low neuronal metabolism during isoflurane-induced burst suppression is related to synaptic inhibition while neurovascular coupling and mitochondrial function remain intact. Clemens Reiffurth 5, 12. https://doi.org/10.1177/0271678X211010353.

Brophy, G.M., Bell, R., Claassen, J., Alldredge, B., Bleck, T.P., Glauser, T., Laroche, S.M., Riviello, J.J., Shutter, L., Sperling, M.R., Treiman, D.M., Vespa, P.M., 2012. Guidelines for the evaluation and management of status epilepticus. Neurocrit. Care. https://doi.org/10.1007/s12028-012-9695-z.

Chalia, M., Lee, C.W., Dempsey, L.A., Edwards, A.D., Singh, H., Michell, A.W., Everdell, N.L., Hill, R.W., Hebden, J.C., Austin, T., Cooper, R.J., 2016. Hemodynamic response to burst-suppressed and discontinuous electroencephalography activity in infants with hypoxic ischemic encephalopathy. Neurophotonics 3 (03), 1. https://doi.org/10.1117/1.NPh.3.3.031408.

Ching, S., Purdon, P.L., Vijayan, S., Kopell, N.J., Brown, E.N., 2012. A neurophysiological-metabolic model for burst suppression. Proc. Natl. Acad. Sci. U. S. A. 109 (8), 3095–3100. https://doi.org/10.1073/pnas.1121461109.

Claassen, J., 2009. How i treat patients with EEG patterns on the ictal-interictal continuum in the neuro ICU. Neurocrit. Care 11, 437–444. https://doi.org/10.1007/s12028-009-9295-8.

Connolly, M., Vespa, P., Pouratian, N., Gonzalez, N.R., Hu, X., 2015. Characterization of the relationship between intracranial pressure and electroencephalographic monitoring in burst-suppressed patients. Neurocrit. Care 22 (2), 212–220. https://doi.org/10.1007/s12028-014-0059-8.

Cormier, J., Maciel, C., Gilmore, E., 2017. Ictal-Interictal continuum: when to worry about the continuous electroencephalography pattern. Semin. Respir. Crit. Care Med. 38 (06), 793–806. https://doi.org/10.1055/s-0037-1607987.

Custo, A., Boas, D.A., Tsuzuki, D., Dan, I., Mesquita, R., Fischl, B., Grimson, W.E.L., Wells, W., 2010. Anatomical atlas-guided diffuse optical tomography of brain activation. Neuroimage 49 (1), 561–567. https://doi.org/10.1016/j.neuroimage.2009.07.033.

Diaz, G.A., Cesaron, E., Alfonso, I., Dunoyer, C., Yaylali, I., 2006. Near infrared spectroscopy in the management of status epilepticus in a young infant. Eur. J. Paediatr. Neurol. 10 (1), 19–21. https://doi.org/10.1016/j.ejpn.2005.11.001.

Doyle, P.W., Matta, B.F., 1999. Burst suppression or isoelectric encephalogram for cerebral protection: evidence from metabolic suppression studies. Br. J. Anaesth. 83 (4), 580–584. https://doi.org/10.1093/bja/83.4.580.

Ferron, J.-F., Kroeger, D., Chever, O., Amzica, F., 2009. Cortical inhibition during burst suppression induced with isoflurane anesthesia. J. Neurosci. 29 (31), 9850–9860. https://doi.org/10.1523/JNEUROSCI.5176-08.2009.

Giorni, C., Di Chiara, L., Cilio, M.R., Ricci, Z., Morelli, S., Garisto, C., Picardo, S., 2009. The usefulness of near-infrared spectroscopy for detecting and monitoring status epilepticus after pediatric cardiac surgery. J. Cardiothorac. Vasc. Anesth. 23 (5), 668–671. https://doi.org/10.1053/j.jvca.2008.12.004.

Haginoya, K., Munakata, M., Kato, R., Yokoyama, H., Ishizuka, M., Iinuma, K., 2002. Ictal cerebral haemodynamics of childhood epilepsy measured with near-infrared spectrophotometry. Brain 125, 1960–1971. https://doi.org/10.1093/brain/awf213.

Hauf, M., Slotboom, J., Nirkko, A., von Bredow, F., Ozdoba, C., Wiest, R., 2009. Cortical regional hyperperfusion in nonconvulsive status epilepticus measured by dynamic brain perfusion CT. Am. J. Neuroradiol. 30 (4), 693–698. https://doi.org/10.3174/ajnr.A1456.

Herlopian, A., Struck, A.F., Rosenthal, E., Westover, B.M., 2018. Neuroimaging correlates of periodic discharges. J. Clin. Neurophysiol. 35 (4), 279–294. https://doi.org/10.1097/WNP.0000000000000466.

Hirsch, L.J., LaRoche, S.M., Gaspard, N., Gerard, E., Svoronos, A., Herman, S.T., Mani, R., Arif, H., Jette, N., Minazad, Y., Kerrigan, J.F., Vespa, P., Hantus, S., Claassen, J., Young, G.B., So, E., Kaplan, P.W., Nuwer, M.R., Fountain, N.B., Drislane, F.W., 2013. American clinical neurophysiology society's standardized critical care EEG terminology. J. Clin. Neurophysiol. 30, 1–27. https://doi.org/10.1097/WNP.0b013e3182784729.

Huppert, T.J., Diamond, S.G., Franceschini, M.A., Boas, D.A., 2009. HomER: a review of time-series analysis methods for near-infrared spectroscopy of the brain. Appl. Opt. 48 (10), D280. https://doi.org/10.1364/AO.48.00D280.

Hurth, H., Schlak, D., Ebner, F.H., 2020. Microdialysis findings in a patient with new onset refractory non-convulsive status epilepticus. Neurocrit. Care 32 (3), 889–893. https://doi.org/10.1007/s12028-019-00848-8.

Kassab, A., Le Lan, J., Tremblay, J., Vannasing, P., Dehbozorgi, M., Pouliot, P., Gallagher, A., Lesage, F., Sawan, M., Nguyen, D.K., 2018. Multichannel wearable fNIRS-EEG system for long-term clinical monitoring. Hum. Brain Mapp. 39 (1), 7–23. https://doi.org/10.1002/hbm.23849.

Kutluay, E., Beattie, J., Passaro, E.A., Edwards, J.C., Minecan, D., Milling, C., Selwa, L., Beydoun, A., 2005. Diagnostic and localizing value of ictal SPECT in patients with nonconvulsive status epilepticus. Epilepsy Behav. 6 (2), 212–217. https://doi.org/10.1016/j.yebeh.2004.12.001.

Lazeyras, F., Blanke, O., Perrig, S., Zimine, I., Golay, X., Delavelle, J., Michel, C.M., De Tribolet, N., Villemure, J.G., Seeck, M., 2000. EEG-triggered functional MRI in patients with pharmacoresistant epilepsy. J. Magn. Reson. Imaging 12, 177–185. https://doi.org/10.1002/1522-2586(200007)12:1<177::AID-JMRI20>3.0.CO;2-3.

Lee, K., Bohnert, S., Wu, Y., Vair, C., Mikler, J., Campbell Teskey, G., Dunn, J.F., 2018. Assessment of brain oxygenation imbalance following soman exposure in rats. Neurotoxicology 65, 28–37. https://doi.org/10.1016/j.neuro.2018.01.007.

Leitinger, M., Trinka, E., Zimmermann, G., Beniczky, S., 2019. Salzburg criteria for nonconvulsive status epilepticus: details matter. Epilepsia 60 (11), 2334–2336. https://doi.org/10.1111/epi.v60.1110.1111/epi.16361.

Lewis, L.D., Ching, S.N., Weiner, V.S., Peterfreund, R.A., Eskandar, E.N., Cash, S.S., Brown, E.N., Purdon, P.L., 2013. Local cortical dynamics of burst suppression in the anaesthetized brain. Brain 136, 2727–2737. https://doi.org/10.1093/brain/awt174.

Liu, X., Zhu, X.-H., Zhang, Y., Chen, W., 2011. Neural origin of spontaneous hemodynamic fluctuations in rats under burst-suppression anesthesia condition. Cereb. Cortex 21 (2), 374–384. https://doi.org/10.1093/cercor/bhq105.

Lührs, M., Goebel, R., 2017. Turbo-Satori: a neurofeedback and brain–computer interface toolbox for real-time functional near-infrared spectroscopy. Neurophotonics 4 (04), 1. https://doi.org/10.1117/1.NPh.4.4.041504.

MÄkiranta, M.J., Jauhiainen, J.P.T., Oikarinen, J.T., Suominen, K., Tervonen, O., Alahuhta, S., JÄntti, V., 2002. Functional magnetic resonance imaging of swine brain during change in thiopental anesthesia into EEG burst-suppression level — A preliminary study. Magma Magn. Reson. Mater. Phys. Biol. Med. 15 (1-3), 27–35. https://doi.org/10.1007/BF02693841.

Marshall, G.T., James, R.F., Landman, M.P., O'Neill, P.J., Cotton, B.A., Hansen, E.N., Morris, J.A., May, A.K., 2010. Pentobarbital coma for refractory intra-cranial hypertension after severe traumatic brain injury: Mortality predictions and one-year outcomes in 55 patients. J. Trauma – Inj. Infect. Crit. Care 69, 275–283. https://doi.org/10.1097/TA.0b013e3181de74c7.

Martini, S., Paoletti, V., Faldella, G., Corvaglia, L., 2019. Cerebral oxygenation patterns during electroclinical neonatal seizures. Neuropediatrics 50 (06), 408–409. https://doi.org/10.1055/s-0039-1693058.

Monrad, P., Sannagowdara, K., Bozarth, X., Bhosrekar, S., Hecox, K., Nwosu, M., Schwabe, M., Meyer, M., Szabo, A., Prigge, J., Lemke, R., Horn, B., Whelan, H.T., 2015. Haemodynamic response associated with both ictal and interictal epileptiform activity using simultaneous video electroencephalography/near infrared spectroscopy in a within-subject study. J. Near Infrared Spectrosc. 23 (4), 209–218. https://doi.org/10.1255/jnirs.1170.

Obrig, H., Neufang, M., Wenzel, R., Kohl, M., Steinbrink, J., Einhäupl, K., Villringer, A., 2000. Spontaneous low frequency oscillations of cerebral hemodynamics and metabolism in human adults. Neuroimage 12 (6), 623–639. https://doi.org/10.1006/nimg.2000.0657.

Peng, K., Nguyen, D.K., Vannasing, P., Tremblay, J., Lesage, F., Pouliot, P., 2016. Using patient-specific hemodynamic response function in epileptic spike analysis of human epilepsy: a study based on EEG-fNIRS. Neuroimage 126, 239–255. https://doi.org/10.1016/j.neuroimage.2015.11.045.

Pisano, A., Di Fraja, D., Palmieri, C., 2020. Monitoring cerebral oximetry by near-infrared spectroscopy (NIRS). In: Anesthesia and Critical Care: Progress and

Perspectives, in: Neuromethods. Humana Press Inc., pp. 75–96. https://doi.org/10.1007/978-1-4939-9891-3_4
Pohlmann-Eden, B., Hoch, D.B., Cochius, J.I., Chiappa, K.H., 1996. Periodic lateralized epileptiform discharges – A critical review. J. Clin. Neurophysiol. 13 (6), 519–530. https://doi.org/10.1097/00004691-199611000-00007.
Pouliot, P., Tremblay, J., Robert, M., Vannasing, P., Lepore, F., Lassonde, M., Sawan, M., Nguyen, D.K., Lesage, F., 2012. Nonlinear hemodynamic responses in human epilepsy: a multimodal analysis with fNIRS-EEG and fMRI-EEG. J. Neurosci. Meth. 204 (2) https://doi.org/10.1016/j.jneumeth.2011.11.016.
Roche-Labarbe, N., Wallois, F., Ponchel, E., Kongolo, G., Grebe, R., 2007. Coupled oxygenation oscillation measured by NIRS and intermittent cerebral activation on EEG in premature infants. Neuroimage 36 (3), 718–727. https://doi.org/10.1016/j.neuroimage.2007.04.002.
Rostrup, E., Law, I., Pott, F., Ide, K., Knudsen, G.M., 2002. Cerebral hemodynamics measured with simultaneous PET and near-infrared spectroscopy in humans. Brain Res. 954 (2), 183–193. https://doi.org/10.1016/S0006-8993(02)03246-8.
Sakakibara, E., Takahashi, Y., Murata, Y., Taniguchi, G., Sone, D., Watanabe, M., 2014. Chronic periodic lateralised epileptic discharges and anti-N-methyl-D- aspartate receptor antibodies. Epileptic Disord. https://doi.org/10.1684/epd.2014.0655.
Scholkmann, F., Kleiser, S., Metz, A.J., Zimmermann, R., Mata Pavia, J., Wolf, U., Wolf, M., 2014. A review on continuous wave functional near-infrared spectroscopy and imaging instrumentation and methodology. Neuroimage 85, 6–27. https://doi.org/10.1016/j.neuroimage.2013.05.004.
Shimogawa, T., Morioka, T., Sayama, T., Haga, S., Kanazawa, Y., Murao, K., Arakawa, S., Sakata, A., Iihara, K., 2017. The initial use of arterial spin labeling perfusion and diffusion-weighted magnetic resonance images in the diagnosis of nonconvulsive partial status epileptics. Epilepsy Res. 129, 162–173. https://doi.org/10.1016/j.eplepsyres.2016.12.008.
Siclari, F., Prior, J.O., Rossetti, A.O., 2013. Ictal cerebral positron emission tomography (PET) in focal status epilepticus. Epilepsy Res. 105 (3), 356–361. https://doi.org/10.1016/j.eplepsyres.2013.03.006.
Strohm, T., Steriade, C., Wu, G., Hantus, S., Rae-Grant, A., Larvie, M., 2019. FDG-PET and MRI in the evolution of new-onset refractory status epilepticus. Am. J. Neuroradiol. 40 (2), 238–244. https://doi.org/10.3174/ajnr.A5929.
Struck, A.F., Westover, M.B., Hall, L.T., Deck, G.M., Cole, A.J., Rosenthal, E.S., 2016. Metabolic correlates of the ictal-interictal continuum: FDG-PET during continuous EEG. Neurocrit. Care 24 (3), 324–331. https://doi.org/10.1007/s12028-016-0245-y.
Sutin, J., Chang, C., Boas, D., Brown, E., Franceschini, M.A., 2014. Diffuse Optical Spectroscopy Measurement Of Cerebral Hemodynamics And Oxygen Metabolism During Anesthesia-Induced Burst Suppression In Rats, in: Biomedical Optics 2014 (2014), Paper BT5B.3. The Optical Society, p. BT5B.3. https://doi.org/10.1364/biomed.2014.bt5b.3.
Vespa, P.M., Miller, C., McArthur, D., Eliseo, M., Etchepare, M., Hirt, D., Glenn, T.C., Martin, N., Hovda, D., 2007. Nonconvulsive electrographic seizures after traumatic brain injury result in a delayed, prolonged increase in intracranial pressure and metabolic crisis. Crit. Care Med. 35 (12), 2830–2836. https://doi.org/10.1097/01.CCM.0000295667.66853.BC.
Vespa, P., Tubi, M., Claassen, J., Buitrago-Blanco, M., McArthur, D., Velazquez, A.G., Tu, B., Prins, M., Nuwer, M., 2016. Metabolic crisis occurs with seizures and periodic discharges after brain trauma. Ann. Neurol. 79 (4), 579–590. https://doi.org/10.1002/ana.v79.410.1002/ana.24606.
Virtanen, J., Noponen, T., Meriläinen, P., 2009. Comparison of principal and independent component analysis in removing extracerebral interference from near-infrared spectroscopy signals. J. Biomed. Opt. 14 (5) https://doi.org/10.1117/1.3253323.
Witsch, J., Frey, H.P., Schmidt, J.M., Velazquez, A., Falo, C.M., Reznik, M., Roh, D., Agarwal, S., Park, S., Connolly, E.S., Claassen, J., 2017. Electroencephalographic periodic discharges and frequency-dependent brain tissue hypoxia in acute brain injury. JAMA Neurol. 74, 301–309. https://doi.org/10.1001/jamaneurol.2016.5325.
Yennu, A., Tian, F., Gatchel, R.J., Liu, H., 2016. Prefrontal hemodynamic mapping by functional near-infrared spectroscopy in response to thermal stimulations over three body sites. Neurophotonics 3 (4), 045008. https://doi.org/10.1117/1.NPh.3.4.045008.
Young, G.B., Mantia, J., 2017. Continuous EEG monitoring in the intensive care unit, in: Handbook of Clinical Neurology. Elsevier B.V., pp. 107–116. https://doi.org/10.1016/B978-0-444-63600-3.00007-6.
Yücel, M.A., Selb, J., Boas, D.A., Cash, S.S., Cooper, R.J., 2014. Reducing motion artifacts for long-term clinical NIRS monitoring using collodion-fixed prism-based optical fibers. Neuroimage 85, 192–201. https://doi.org/10.1016/j.neuroimage.2013.06.054.
Zhang, Y., Brooks, D., Franceschini, M.A., Boas, D.A., 2005. Eigenvector-based spatial filtering for reduction of physiological interference in diffuse optical imaging. J. Biomed. Opt. 10 (1) https://doi.org/10.1117/1.1852552.
Zubler, F., Steimer, A., Gast, H., Schindler, K.A., 2014. Seizure termination, in: International Review of Neurobiology. Academic Press Inc., pp. 187–207. https://doi.org/10.1016/B978-0-12-418693-4.00008-X.